

R-FFT: Function Split at IFFT/FFT in Unified LTE CRAN and Cable Access Network

Akhilesh S. Thyagaturu, Ziyad Alharbi, and Martin Reisslein

Abstract—The Remote-PHY (R-PHY) modular cable network for Data over Cable Service Interface Specification (DOCSIS) service conducts the physical layer processing for the transmissions over the broadcast cable in a remote node. In contrast, the cloud radio access network (CRAN) for Long-Term Evolution (LTE) cellular wireless services conducts all baseband physical layer processing in a central baseband unit and the remaining physical layer processing steps towards radio frequency (RF) transmission in remote nodes. Both DOCSIS and LTE are based on Orthogonal Frequency Division Multiplexing (OFDM) physical layer processing. We propose to unify cable and wireless cellular access networks by utilizing the hybrid fiber-coax (HFC) cable network infrastructure as fiber fronthaul network for cellular wireless services. For efficient operation of such a unified access network, we propose a novel Remote-FFT (R-FFT) node that conducts the physical layer processing from the Fast-Fourier Transform (FFT) module towards the RF transmission, whereby DOCSIS and LTE share a common FFT module. The frequency domain in-phase and quadrature (I/Q) symbols for both DOCSIS and LTE are transmitted over the fiber between remote node and cable headend, where the remaining physical layer processing is conducted. We further propose to cache repetitive quadrature amplitude modulation (QAM) symbols in the R-FFT node to reduce the fronthaul bitrate requirements and enable statistical multiplexing. We evaluate the fronthaul bitrate reductions achieved by R-FFT node caching, the fronthaul transmission bitrates arising from the unified DOCSIS and LTE service, and illustrate the delay implications of moving part of the cable R-PHY remote node physical layer processing to the headend. Overall, our evaluations indicate that the proposed R-FFT node can effectively support unified DOCSIS and LTE services over the HFC cable plant while substantially reducing the fronthaul bitrate requirements of the existing CRAN structures.

Index Terms—Broadcast cable, Cable access network, Cellular wireless network, Delay, DOCSIS, Internet access.

I. INTRODUCTION

A. Motivation: Modular Cable DOCSIS and Cellular LTE Architectures

The architectures of both the broadcast cable DOCSIS access network and the cellular wireless LTE access network have recently been evolving towards modular architectures. In broadcast cable networks, the Modular Headend Architecture version 2 (MHA_{v2}) [1] implements the Cable Modem Termination System (CMTS) functions in a modular fashion. Specifically, in the R-PHY architecture [2]–[4], a digital fiber

links the headend with distributed Remote PHY nodes (RPDs). An RPD can be located close to the cable modems (CMs), improving the signal quality on the broadcast cable. The RPD conducts all the physical layer processing for the transmissions to and from the CMs, while the higher layer processing is conducted centrally at the headend.

Similarly, in cellular wireless access, the Cloud Radio Access Network (CRAN) architecture splits communication functions between centralized Base Band Units (BBUs) that conduct the baseband signal processing and Remote Radio Units (RRUs), which conduct the passband processing for the physical RF transmissions. A central BBU can support multiple RRUs and thus provide a common platform for centralized resource management. BBUs are typically flexibly implemented in software on generic computing hardware [5], [6] and are amenable to implementation on cloud computing resources. Also, conducting the baseband processing in the BBU reduces the complexity and cost of the RRUs, which is particularly advantageous for large-scale small cell deployments.

Importantly, both DOCSIS 3.1 [7] and LTE are based on OFDM physical layer processing, which requires an IFFT/FFT module as main last step of the baseband processing. In the downstream direction, the FFT module produces the time domain I/Q samples that the LTE CRAN transports over the fronthaul link from BBU to RRUs.

B. Challenge: Fronthaul for CRAN

A critical challenge of CRAN operation is the fronthaul transport of the time domain I/Q samples between BBU and RRUs, which require low latency and high bitrates [8]. A low-latency high-bitrate connection must constantly be maintained between BBU and RRUs, regardless of the actual user traffic. That is, the analog RF signals must be transmitted and received at all times, even when there is no wireless user activity. For instance, the passband signal with the cell broadcast information and reference or pilot tones must always be transmitted. Thus, the I/Q samples of the RF passband must be transported at the constant rate at all times. Moreover, the transmission requirements over the optical fiber increase linearly with the number of remote nodes. Therefore, numerous techniques, such as [9]–[12], have been proposed to dynamically compress the RF I/Q samples for effective transmissions over the optical fiber. However, the compression techniques are lossy because of the RF signal quantization, reducing the sensitivity of the receiver in the upstream. Nevertheless, the data rate requirements between BBU and RRUs typically lead to dedicated costly

Please direct correspondence to M. Reisslein.

A. Thyagaturu, Z. Alharbi, and M. Reisslein are with the School of Electrical, Computer, and Energy Eng., Arizona State Univ., Tempe, AZ 85287-5706, USA (e-mail: {athyagat, zalharbi, reisslein}@asu.edu).

Z. Alharbi is also with the King Abdulaziz City for Science and Technology, Riyadh, Saudi Arabia, (e-mail: zalharbi@kacst.edu.sa).

deployments of optical fiber connections and static allocations of transmission resources.

C. Solution: Unify Cable DOCSIS and CRAN LTE Networks

We address the LTE CRAN fronthaul challenge by exploiting the fiber capacity between the cable headend and the cable remote nodes in the installed hybrid fiber-broadcast coax networks. In particular, we propose a novel Remote-FFT (R-FFT) architecture, see Section III, that co-locates the LTE RRUs with the cable remote nodes, while the LTE BBUs are co-located with the cable headends (or outsourced to a cloud resource). The R-FFT node includes the IFFT/FFT module as well as the conventional RRU processing modules towards the RF transmission. Both cable DOCSIS and wireless LTE share the IFFT/FFT module in the R-FFT node. Thus, both DOCSIS and LTE frequency domain I/Q samples are transported over the fiber link between cable headend and remote nodes. In order to further reduce the fronthaul bitrates in the downstream direction, we propose to cache repetitive QAM symbols in the remote nodes in Section IV. Our evaluations in Section V present the bitrate reductions achieved by the QAM symbol caching in the remote node. We also evaluate the fronthaul bitrates required for the unified DOCSIS and LTE operation and the delay implications of the transition of an existing R-PHY cable remote node to an R-FFT remote node.

D. Related Work

Our study relates to modular access network strategies that have so far mainly been studied in isolation for broadcast cable networks and for wireless cellular networks as well as to caching strategies in access networks. Broadcast cable access networks have been extensively studied for providing wired broadband Internet access to residential users [13]–[22]. Recent studies have examined the impact of the distance between the remote node and cable headend on the medium access control (MAC) performance of the R-PHY modular architecture (which conducts all physical layer processing in the remote node and the MAC in the headend) and the R-MACPHY architecture (which conducts all physical layer processing plus the MAC in the remote node) [2], [4]. The studies found that the modular R-PHY architecture gives good throughput-delay performance for short headend-to-remote node distances up to around 100 km. We consider the R-PHY modular architecture as starting point for our R-FFT node development and move some of the physical layer processing to the headend.

A very extensive set of literature has examined modular wireless cellular access network architectures. Extensive CRAN studies have demonstrated the advantages and challenges of conducting the LTE physical layer baseband processing in the BBU [23]–[29]. The high transmission bitrate requirements for transporting the time-domain I/Q samples produced by the baseband processing at the BBU to the RRU have spurred research on fronthaul transport strategies, see e.g., [30]–[32], and alternative function splits between BBU and RRU [8], [33]–[42]. Complementary to this extensive research, which has examined cellular wireless access in an

isolated manner and typically considered abstract models for the fronthaul between BBU and RRU, we propose to unify cable and wireless access networks. More specifically, we pursue a specific function split at the IFFT/FFT module that (i) reduces the fronthaul transmission bitrate requirements compared to the conventional CRAN time domain I/Q sample transmission, (ii) shares the IFFT/FFT module in the remote node among DOCSIS and LTE, and (iii) shares the fiber infrastructure between cable headends and remote nodes for DOCSIS transport and LTE cellular wireless fronthaul.

Mechanisms to reduce the carbon foot print of access networks have recently been investigated in wireless networks [43]–[49] as well as cable networks [50]–[52]. This line of energy saving research has included studies on the caching of application layer content items in or near the RRUs, e.g., [53]–[55]. In contrast to the caching of application layer content items, we examine the caching of repetitive PHY layer QAM I/Q symbols at the RRU.

Only few studies have explored supporting wireless services with cable networks. In particular, the channel propagation characteristics of indoor femto cells that are supported over cable links have been modeled in [56], [57]. The economic benefits of general infrastructure sharing by residential wired and cellular wireless networks have been explored in [58]. The economic benefits of integrating LTE and DOCSIS have been discussed in [59], [60], while general fiber cost sharing has been studied in [61]. We note for completeness that the application layer performance of LTE wireless access has been compared with wired DOCSIS access in [62]; however, the study [62] did not seek to unify LTE and DOCSIS networks. In contrast to the existing studies, we seek to efficiently unify DOCSIS cable and LTE wireless access networks through the sharing of the cable headend-to-remote node fiber infrastructure and the sharing of the IFFT/FFT module in the remote node. At the same time, the PHY layer function split at the IFFT/FFT module reduces the high fronthaul bitrate requirements of the conventional CRAN with PHY layer baseband processing at the BBU, while still allowing for extensive softwarized physical layer processing at the BBU or headend.

II. BACKGROUND ON FUNCTION SPLITS IN LTE AND CABLE NETWORKS

A. Wireless Downstream vs. Upstream Transmissions

1) *Upstream*: In the upstream direction, the RRU receives the RF signal transmitted from the users. This analog passband signal is down-converted to the baseband and digitized for the transmission to the BBU for baseband processing. Unlike the cable link in traditional cellular networks and antenna infrastructures, the CRAN connects the BBU and RRU with a digital optical fiber. The cable link in traditional infrastructures added significant attenuation to the upstream signal, which is especially harmful due to the low signal levels received from the user devices. In contrast, the digital fiber does not contribute towards the attenuation loss as it carries the signal in digital form. Extreme care is needed at the RRUs for digitizing the uplink signal from the users as any additional loss should

be avoided due to the low level of the uplink RF signal at the RRU. For example, if the cable link accounts for 2 dB of loss and the noise floor is -120 dB, then the received signal at the RRU connected to a BBU over a cable link must be ≥ -118 dB for successful detection. The received signal can be as low as -120 dB if the RRU is connected to a BBU through a digital fronthaul link, thus the digital fronthaul link increases the dynamic range of the system by 2 dB. The Single Carrier Orthogonal Frequency Division Multiplexing (SC-OFDM) uplink modulation format is used in typical current deployments. However, SC-OFDM requires a Discrete Fourier Transform (DFT) just before the FFT computation, so as to spread an I/Q sample across multiple FFT input channels. This DFT spreading, while ensuring good noise resilience, is a complex operation. Also, SC-OFDM has spectral inefficiencies. Therefore, technology is advancing towards uplink OFDM systems where the complex preprocessing of the discrete Fourier transform (DFT) before FFT computations can be eliminated, especially for MIMO applications [63], [64]. Therefore, we focus on symmetrical OFDM systems in both the upstream and downstream directions in this article. The processing of the upstream signals for the detection and extraction of information from the RF uplink signals can be centrally executed in the cloud based BBU on generic hardware, such as the general purpose processors.

2) *Downstream*: In the downstream direction, the BBU sends the information to the RRUs for the generation of the passband signal to transmit over the physical antennas. The RRUs can easily set the transmit power level gain states for RF signals. In contrast to the upstream direction, there is no significant difference in terms of power level of the signal generation or the dynamic range of the systems between cable and digital fronthaul links. Similar to the centralized processing of the upstream in the cloud based BBU, the information is centrally processed on generic hardware, such as general purpose processors, to generate the baseband downstream signals.

B. Function Split in LTE

Figure 1 shows the conventional CRAN deployment in comparison to traditional cellular deployments. A radio base station protocol stack, e.g., the LTE protocol stack at the eNB towards the UE, can be functionally split and implemented flexibly over radio remote node and BBU. The conventional CRAN transports the baseband time domain I/Q samples over optical fiber to the RRUs. The number of supported RRUs is limited by the amount of traffic over the optical fiber. Let R_o [bit/s] denote the capacity of the fronthaul optical connectivity and R_u denote the data rate required by RRU u . Then, the maximum number of RRUs N that can be supported over the fronthaul link is the largest N such that $\sum_{u=1}^N R_u \leq R_o$. In present CRAN deployments, the fronthaul link resources are typically statically allocated. Therefore in symmetrical and homogeneous deployments with equal RRU data rates, i.e., $R_1 = R_2 = \dots = R_N = R_{\bar{u}}$, the fronthaul link can support at most $N = R_o/R_{\bar{u}}$ RRUs. The main bottleneck for CRAN deployments is the delay and capacity of the fronthaul link.

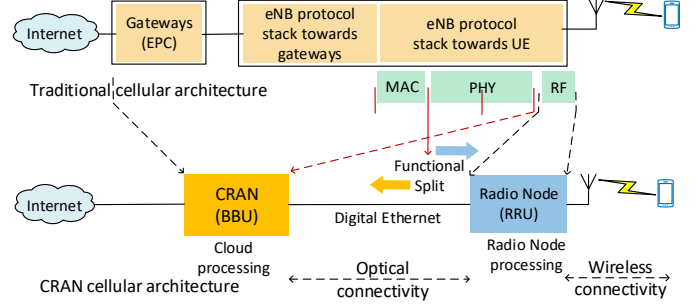


Fig. 1. The Cloud RAN (CRAN) implements the RAN functions on the cloud-based Baseband Unit (BBU), where baseband signals are processed and digital information is transmitted to a remote radio node, the Remote Radio Unit (RRU). The RRU generates the passband signal for the physical transmission of the wireless RF signal over the antenna. The RAN protocol stack towards the UE, especially at the MAC and PHY layers can be flexibly split between BBU and RRU to relax the data rate and latency constraints on the optical fiber.

TABLE I
SUMMARY OF MAIN NOTATIONS

| Transmission bitrates | |
|---|---|
| R_C | Cable DOCSIS transmission bitrate (capacity) [bps] |
| ρ_C | Cable payload traffic intensity (load) [unit-free], corresp. bitrate is $\rho_C \cdot R_C$ |
| R_L | Wireless LTE transmission bitrate (capacity) [bps] |
| ρ_L | LTE payload traffic intensity (load) [unit-free], corresp. bitrate is $\rho_L \cdot R_L$ |
| R^P | Passband bitrate [bps] |
| R^B | Baseband time domain I/Q bitrate [bps] |
| R^F | Baseband frequency domain I/Q bitrate [bps] |
| R_o | Transm. bitrate (capacity) of opt. fiber between headend and remote node |
| ρ_B | Traffic intensity from baseband time domain I/Q samples, relative to R_o |
| LTE CRAN parameters with typical settings | |
| N | Number of RRUs per CRAN BBU, $N = 1$ |
| B_{sub} | Number of subcarriers, $B_{\text{sub}} = 1200$ |
| K | Bits per \Re/\Im of I/Q sample, $K = 10$ bits |
| W | Number of Tx/Rx antennas, $W = 1$ |
| T_s | OFDM symbol duration, $T_s = 66.6 \mu\text{s}$ |
| f_s | Sampling frequency, $f_s = 30.72$ MHz |
| f_c | Carrier frequency, $f_c = 2$ GHz |

To understand the RRU fronthaul requirements, we estimate the data rates required by the conventional CRAN, where the baseband I/Q samples are transported from the BBU to the RRU, which is the most common LTE deployment scenario. General data rate comparisons of various function split approaches in the LTE protocol stack have been conducted in [8], [35], [36]. Complementary to these existing evaluations, we closely examine the data rate requirements based on the implementation specifics of the protocol stack. That is, we track the information flows across multiple LTE protocol stack layers and identify the key characteristics that govern the fronthaul link requirements. Based on the computationally intensive FFT operation, the data flow between BBU and RRU can be categorized into two types: 1) time domain samples, and 2) frequency domain samples. Table I summarizes the main parameters for the evaluation of the fronthaul optical link requirements connecting RRU and BBU in the LTE context. We consider in the following evaluations an LTE system with 20 MHz system bandwidth, which has an $f_s = 30.72$ MHz

sampling frequency and can support an LTE transmission bit rate of $R_L = 70$ Mbps.

1) *Time Domain I/Q Sample Forwarding*: The time domain I/Q samples represent the RF signal in the digital form either in the passband or the baseband. The digital representation of the passband signal requires a very high data rate that depends on the physical transmission frequency band. Thus, passband time domain I/Q sample forwarding is usually non-economical. For example, in an LTE system, the passband signal is sampled at twice the carrier frequency f_c , with each sample requiring $K = 10$ bits for digital representation. Although the LTE deployment norm is to use $W = 2$ or more eNB antennas, for clarity and simplified comparison of multiple function split mechanisms, we set the number of antennas to $W = 1$. The resulting passband I/Q data rate over the fronthaul link is

$$\begin{aligned} R^P &= N \times W \times 2 \cdot f_c \times K \\ &= 1 \times 1 \times 2 \cdot 2 \cdot 10^9 \text{ Hz} \times 10 \text{ bit} = 40 \text{ Gbps.} \end{aligned} \quad (1)$$

The baseband signal for an OFDM symbol in the time-domain consists of a number of time samples equal to the number of OFDM subcarriers because of the symmetric input and output samples of the IFFT/FFT structure. A cyclic prefix is added to the OFDM signal to avoid inter-symbol interference. In order to reduce the constraints on the RF signal generation at the RRU, the baseband signal is sampled at a frequency of $f_s = 30.72$ MHz, with each sample requiring $K = 10$ bits for digital representation, and an oversampling factor of 2. The resulting baseband I/Q data rate is

$$\begin{aligned} R^B &= N \times W \times 2 \cdot f_s \times 2 \cdot K \\ &= 1 \times 1 \times 2 \cdot 30.72 \cdot 10^6 \text{ Hz} \times 2 \cdot 10 \text{ bit} \\ &= 1.23 \text{ Gbps.} \end{aligned} \quad (2)$$

Although the baseband I/Q data rate R^B is significantly lower than the passband I/Q rate R^P , the baseband I/Q data rate R^B scales linearly with the number of antennas and the bandwidth. Thus, for large numbers of antennas W and wide aggregated bandwidth, the baseband data rate R^B can be very high.

2) *Frequency Domain I/Q Sample Forwarding*: In a 20 MHz LTE system, the duration T_s of one OFDM symbol, including the cyclic prefix, is $71.4 \mu\text{s}$, which corresponds to 2192 time samples for each T_s . The useful symbol duration in the OFDM symbol duration T_s is $66.7 \mu\text{s}$ or 2048 samples, out of which the cyclic prefix duration is $4.7 \mu\text{s}$ or 144 samples. Thus, each set of 2048 samples in an OFDM symbol (excluding the cyclic prefix) corresponds to $B_{\text{sub}} = 2048$ subcarriers when transformed by the FFT. However, only 1200 of these subcarriers are used for signal transmission, which corresponds to 100 resource blocks (RBs) of 12 subcarriers; the remaining subcarriers are zero-padded and serve as guard carriers. This leads to $(2048 - 1200)/2048 = 0.41 = 41\%$ of unused guard carriers. Each OFDM subcarrier is modulated by a complex value mapped from a QAM alphabet. The LTE QAM alphabet size is based on QAM bits, such as 64 QAM and 256 QAM. The resulting frequency domain subcarrier information data rate R^F is proportional to the number of subcarriers B_{sub} . That is, a vector of complex valued QAM

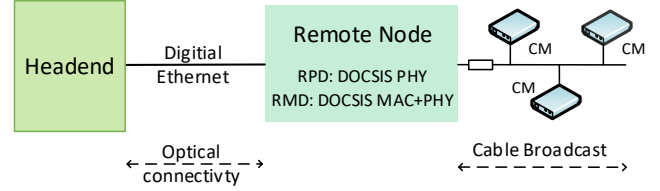


Fig. 2. The Distributed Converged Cable Access Platform (DCCAP) Architecture separates the modular CMTS functions and implements some functions at remote nodes deployed close to the users. A remote node can function as a Remote-PHY Device (RPD) implementing the CMTS DOCSIS PHY, or as a Remote-MACPHY Device (RMD) implementing the DOCSIS MAC and PHY.

alphabet symbols of size B_{sub} needs to be sent once every OFDM symbol duration T_s , resulting in the data rate

$$\begin{aligned} R^F &= N \times W \times B_{\text{sub}} \times T_s^{-1} \times 2 \cdot K \\ &= 1 \times 1 \times 1200 \times (66.7 \cdot 10^{-6} \text{ s})^{-1} \times 2 \cdot 10 \text{ bit} \\ &= 360 \text{ Mbps,} \end{aligned} \quad (3)$$

which is a 70 % reduction compared to the time domain baseband I/Q data rate R^B .

C. Function Split in Cable Distributed Converged Cable Access Platform (DCCAP) Architectures

The traditional HFC network CCAP architecture implements the CMTS at the headend and transports the analog optical signal to a remote node over the optical fiber. The remote node then converts the optical analog signal to an electrical RF signal for transmission over the broadcast cable segment. However, the analog signal is prone to attenuation in both the optical fiber segment as well as the cable segment. If the remote node is deployed far from the headend, then the attenuation of the optical signal will dominate; conversely, if the remote node is deployed far from the CMs (users), then the attenuation of the RF signal in the cable will dominate.

The Modular Headend Architecture (MHA) overcomes the analog optical signal attenuation in the CCAP architecture by splitting the CMTS functions, i.e., by modularizing the implementation of the CMTS functions. The implementation of modular CMTS functions in a distributed manner across multiple nodes results in distributed DCCAP architectures [65], [66]. As shown in Fig. 2, the DCCAP architecture defines a remote node that is connected to the headend through a digital Ethernet fiber. The digital connection between the remote node and the headend eliminates the optical signal attenuation, allowing the remote node to be deployed deep into the HFC network. The remote node deployment deep into the HFC network reduces the cable segment length, which in turn reduces the analog RF signal attenuation and improves the overall Signal to Noise Ratio (SNR) at the CM. The network connecting the remote node to the headend is referred to as Converged Interconnect Network (CIN). The MHA version 2 (MHA v2) [1] architecture defines two DCCAP architectures: Remote-PHY and Remote-MACPHY.

In the R-PHY architecture [1], the DOCSIS PHY functions in the CMTS protocol stack are implemented at the remote node, which is referred to as Remote-PHY Device (RPD).

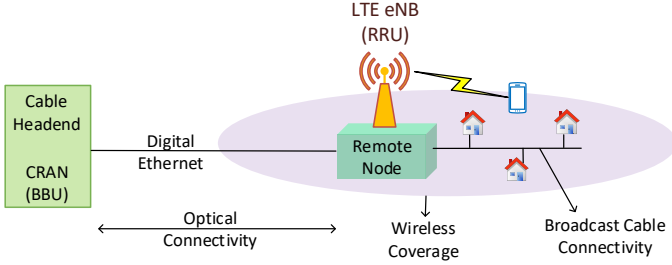


Fig. 3. Proposed unified LTE and cable (HFC) access network architecture: An LTE eNB RRU is deployed at the HFC remote node site. The RRU is connected with the digital optical fiber segment of the HFC network, (which functions now also as the radio access fronthaul link) to the Base Band Unit (BBU). The BBU and the Radio Access Network (RAN) functions are implemented at the cable headend as a cloud RAN (CRAN).

All higher layers in the CMTS protocol stack, including the MAC as well as the upstream scheduler, are implemented at the headend. A virtual-MAC (vMAC) entity can virtualize the DOCSIS MAC on generic hardware, which can be flexibly deployed at either the headend or in a cloud/remote data center. The RPD is simple to implement and hence has low cost.

III. PROPOSED UNIFIED ACCESS NETWORK ARCHITECTURE FOR LTE AND CABLE NETWORKS

The digital optical remote node in the DCCAP architecture is deployed close to the CMs (users). The close proximity of the remote node to the residential subscribers can be exploited for establishing wireless LTE connectivity through deploying an LTE eNB RRU at the remote node site, as illustrated in Fig. 3. With the establishment of LTE connectivity by the cable system operator, users can be wirelessly connected to the cable system core network for Internet connectivity, increasing the cable system service capabilities. The LTE eNB RRU at the remote node reuses the existing HFC infrastructure, enabling cable system operators to provide additional LTE services with low costs.

A. PHY Function Split at IFFT/FFT

LTE and DOCSIS 3.1 share similar PHY transceiver characteristics for the OFDM implementation. We propose to exploit these PHY transceiver similarities to simultaneously support LTE and DOCSIS over the HFC network. The general overview of the physical layer for LTE and DOCSIS is shown in Fig. 4. In the downstream direction, the data from the MAC layer is processed to form PHY frames and mapped to OFDM resource locations, which are then converted to frequency domain QAM I/Q symbols (see Sec. II-B2) based on the modulation and coding schemes. The QAM I/Q symbols are then IFFT transformed to obtain the complex time domain samples. These time domain samples (see Sec. II-B1) are then converted to an analog RF signal for transmission. In a conventional CRAN, the remote node conducts the DAC/ADC and the onward processing steps towards the RF transmission; the conventional CRAN remote node is therefore also referred to as R-DAC/ADC node.

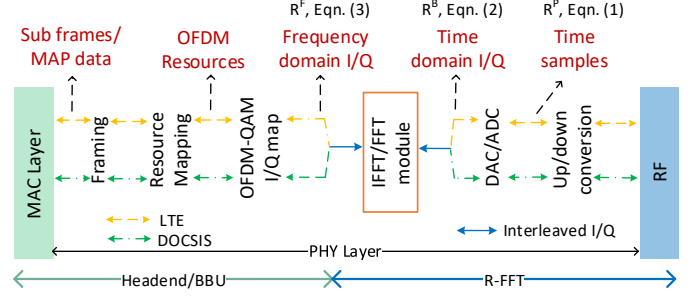


Fig. 4. Wireless LTE and cable DOCSIS 3.1 share the same OFDM physical layer structure. OFDM based physical layer processing can be separated into functions of framing, resource mapping, and OFDM-QAM I/Q mapping, which are conducted separately for DOCSIS and LTE at the headend in the R-FFT architecture. IFFT/FFT processing, Digital to Analog conversion, and passband RF signal up/down conversion are then conducted in the R-FFT node. The MAC layer emanates PHY layer payload traffic bitrates $\rho_L R_L$ for LTE and $\rho_C R_C$ for cable. These payloads are processed in the PHY layer, resulting in the increasingly higher bitrates R^F , R^B , and R^P .

The I/Q information undergoes different DOCSIS and LTE protocol specific processing before (to the left of) the IFFT/FFT module as well as after (to the right of) the IFFT/FFT module. However, the same IFFT/FFT module can be used for the I/Q processing of both DOCSIS and LTE, as illustrated in Fig. 4. Thus, we can separate (split) the functions at the IFFT/FFT module. That is, the IFFT/FFT and the processing steps between IFFT/FFT and RF are implemented at the remote node; whereas the steps towards the MAC layer are implemented at the headend. This function split at the IFFT/FFT node can simultaneously support LTE and DOCSIS over the HFC network.

B. Common IFFT/FFT for LTE and DOCSIS

The LTE and DOCSIS protocols both employ OFDM as the physical layer modulation technique. The OFDM modulation relies on FFT computations [67]. The fact that both LTE and DOCSIS require the same IFFT/FFT computations for each OFDM modulation and demodulation can be exploited by using the same computing infrastructure. The implementation of parallel FFT computations, i.e., FFT computations for multiple protocols, on a single computing infrastructure yields several advantages. Utilizing the same computing infrastructure for the LTE and DOCSIS FFT computations reduces the power consumption and design space [68]–[71].

Thus, the main motivation for computing the FFT at the remote node is to exploit a common remote node platform while flexibly realizing the different OFDM transmission formats for heterogeneous OFDM based protocols at the headend. Figure 5 illustrates the R-FFT remote node architecture for simultaneously supporting cable and LTE. Generally, in the downstream direction, an IFFT operation is performed once for every OFDM symbol duration. The LTE OFDM symbol duration is approximately $T_L = 71.4 \mu\text{s}$, while the DOCSIS OFDM symbol duration is typically either $T_C = 84.13 \mu\text{s}$ or $40 \mu\text{s}$. However, the actual IFFT compute times τ_L and τ_C , for LTE and DOCSIS, respectively, can span from a few microseconds to several tens of microseconds. Consequently,

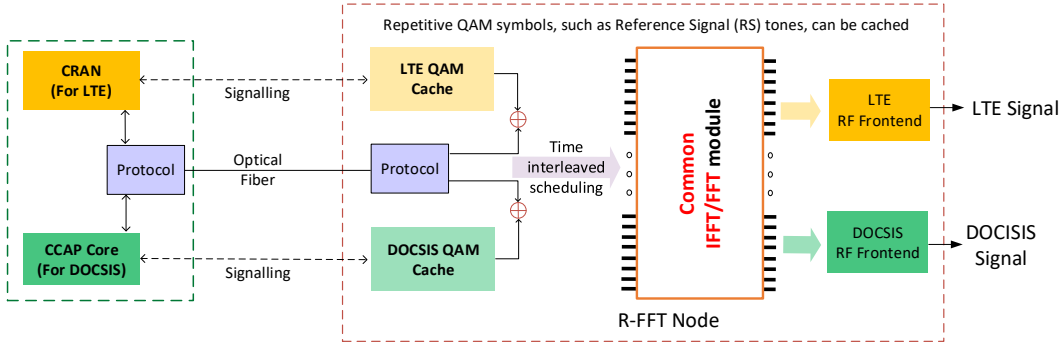


Fig. 5. The cable DOCSIS and LTE IFFT/FFT computations are time interleaved on a common IFFT/FFT module in the R-FFT node. Repetitive DOCSIS and LTE QAM symbols can be cached in the R-FFT node, see Section IV, controlled through a signalling protocol.

there are typically long idle time periods in the IFFT module inbetween the FFT computations. Thus, we can interleave the I/Q input in time such that same IFFT/FFT module can be used for multiple OFDM based technologies, e.g., for LTE and DOCSIS. By reusing the IFFT/FFT computing structures we can reduce the complexity of the hardware, be more power efficient, and reduce the cost of the remote node.

C. Proposed Shared Remote-FFT (R-FFT) Node

In the uplink direction, the proposed R-FFT remote node converts the incoming DOCSIS RF signal from the CMs to an encapsulated data bits format that can be transported over the digital fiber link for additional processing and onward forwarding at the headend. In a similar way, in the downstream direction, RF signals are generated from the incoming formatted data bits and sent out on the RF cable link to the CMs. For LTE, an eNB can use a wide range of licensed spectrum with a single largest carrier component of 20 MHz; the bandwidth can be further extended by carrier aggregation techniques to obtain larger effective bandwidths. The R-FFT node effectively converts the upstream LTE RF signal from the wireless users to a digital signal for transport over the digital fiber link to the BBU/CRAN. In the downstream direction, the R-FFT node converts the digital information to an LTE RF signal for wireless transmission to the users.

We address the high fiber data rate in conventional CRANs through a balanced split among the functions within the PHY layer while keeping the remote node simple. The R-DAC/ADC node in existing conventional CRANs requires some digital circuitry, such as a CPU, for the DAC and ADC control. The FFT/IFFT can be implemented very efficiently [72], [73] so that existing DAC/ADC remote nodes can take over the FFT/IFFT with relatively modest modifications or without modifications if the remote node has enough spare computing capacity. The advantages of the proposed FFT implementation at the remote node include:

- i) flexible deployment support for LTE and DOCSIS
- ii) requires lower data rate R^F , see Eqn. (3), to transport frequency domain I/Q samples as compared to time-domain I/Q samples, which require the higher R^B rate, see Eqn. (2).
- iii) data tones carrying no information are zero valued in the frequency I/Q samples, effectively lowering the data-rate

over the fiber channel for both LTE and DOCSIS, thus enabling statistical multiplexing, and

- iv) possible caching of repetitive frequency QAM I/Q samples, such as Reference Signals (RS) and pilot tones.

We emphasize that in the proposed R-FFT system, the data rate required over the fiber is directly proportional to the user traffic. We believe this is an important characteristic of the FFT function split whereby we can achieve multiplexing gains by combining multiple R-FFT nodes, each supporting DOCSIS and LTE services, as illustrated in Fig. 3. In addition, the proposed mechanism enables the implementation of the complex PHY layer signal processing at the headend. Examples of the signal processing operations include channel estimation, equalization, and signal recovery, which can be implemented with general-purpose hardware and software. Moreover, the processing of digital bits, such as for low density parity check forward error correction, can be implemented at the headend. Thus, the proposed R-FFT approach reduces the cost of the remote nodes and increases the flexibility of changing the operational technologies. The software implementations at the headend can be easily upgraded while retaining the R-FFT node hardware since the node hardware consists only of common platform hardware, such as elementary DAC/ADC and FFT/IFFT components. Thus, the proposed approach eases technology upgrades. That is, the R-FFT node has minimal impact on technology advancements because the R-FFT blocks are elementary or independent of most technology advances.

D. Interleaving Timing of FFT Computations

In this section we briefly outline the scheduling of the interleaving of IFFT/FFT computations on a single computing resource. Sharing a single IFFT/FFT computing module reduces the capital and operational expenditures for the remote node compared to conducting the DOCSIS and LTE IFFT/FFT computations on two separate IFFT/FFT modules. Nevertheless, we note that it is possible to operate an R-FFT node with two separate FFT/IFFT modules. Such an operation with two FFT/IFFT modules would still benefit from the lower LTE fronthaul bitrates, but would not achieve the expenditure reductions due to sharing a single common IFFT/FFT module.

Figure 6 illustrates the basic timing diagram to schedule the FFT computations on the computing resource for the case where (i) the LTE OFDM symbol duration T_L is longer than

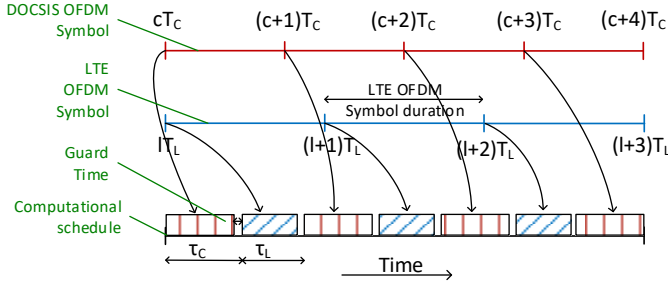


Fig. 6. The IFFT/FFT computations of two heterogeneous OFDM based technologies can be interleaved to use the same computing resource at the remote node: Illustration of the periodic cycle behavior when long LTE OFDM symbol durations T_L are interleaved with short DOCSIS OFDM symbol durations T_C , whereby the DOCSIS FFT computation takes longer than the LTE FFT computation, i.e., $\tau_C > \tau_L$.

the DOCSIS OFDM symbol duration T_C and the DOCSIS FFT computation takes longer than the LTE FFT computation, i.e., $\tau_C > \tau_L$ (due to the larger DOCSIS FFT size compared to the LTE FFT). In Fig. 6, c and l denote the indices for the independent DOCSIS and LTE periodic symbols, which start to arrive simultaneously at the left edge of the drawn scenario. We note that the computation times τ_C and τ_L can include a guard time to account for the context switching between the LTE and DOCSIS technologies. The switching time depends on the FFT size and technology-specific parameters, such as the cyclic prefix duration. The guard time also depends on the memory and CPU functional capabilities and can vary based on specific implementations. For instance, an implementation can include a power savings technique in which the FFT computing module can be operated in “sleep modes”, where, the idle times are power gated to the computing module (i.e., the power supply is completely disconnected from the computing module). Guard times would then need to compensate for the wake-up time (i.e., the transition from a sleep mode to a computation mode) in addition to data load and read [74]–[77]. The resulting guard times will typically be on the order of microseconds, i.e., a small fraction of the typical OFDM symbol durations of 40 and 80 μ secs.

The scheduling of multiple periodic tasks on a shared resource has been extensively studied [78]–[81]. With preemptive scheduling, which may interrupt an ongoing computation task, tasks are schedulable if the sum of the individual ratios of task computation time to task period duration is less than or equal to one [82], i.e., in our context if $\tau_C/T_C + \tau_L/T_L \leq 1$. Non-preemptive scheduling requires an additional condition [83, Theorem 4.1, 2)], which in our example context corresponds to $T_C \geq \tau_L$ in conjunction with $T_L \geq \tau_L + \tau_C$. Non-preemptive scheduling appears better suited for the R-FFT node so as to avoid extra load and read times. Non-preemptive earliest deadline first scheduling (EDF) can schedule the tasks that satisfy these preceding conditions. In particular, we set the deadline for completing the computation of a symbol arriving at time cT_C , resp., lT_L , to be completed by the arrival of the subsequent symbol at time $(c+1)T_C$, resp., $(l+1)T_L$. The non-preemptive EDF scheduler selects always the tasks with the earliest completion deadline

Algorithm 1: Caching and FFT Computation Procedure

1. CRAN/Headend

- (a) Identify cachable I/Q samples. (Secs. IV-A+IV-B)
- (b) Create caching rules. (Secs. IV-A+IV-B)
- (c) Signal the rules and data for caching. (Sec. IV-D)

if *Cached I/Q samples require updating* **then**

 | Signal remote node for cache renew or flush.

end

2. Remote Node

foreach *OFDM Symbol in T_C and T_L* **do**

if *Caching is enabled* **then**

 | Read cache and I/Q mapping;

 | Add cache-read I/Q to received I/Q;

1

end

if *FFT module is free* **then**

 | Schedule I/Q for FFT;

2

end

else

 | Schedule at completion of current execution;

3

end

end

and breaks ties arbitrarily. We note that other schedules could be employed for the relatively simple scheduling of only two interleaved tasks, e.g., an elementary static cyclic schedule [84], [85]. Additionally, scheduling techniques that consider energy-efficiency, e.g., [86]–[89] may be considered. The detailed examination of different scheduling approaches for the proposed R-FFT node is beyond the scope of this study and is an interesting direction for future research.

The sharing of the FFT/IFFT module by multiple technologies can be extended to include both upstream and downstream directions, i.e., the module can be shared by downstream DOCSIS and LTE as well as upstream DOCSIS and LTE, as the computations for the different directions are performed independently of each other, even for wireless full-duplex communications. Also, the FFT computation duration τ can represent the aggregate of multiple OFDM symbol instances. For example, in the case of carrier aggregation in LTE (or channel bonding in DOCSIS), there would be an OFDM symbol for each of the α carrier component, resulting in $\tau_L = \tau_1 + \tau_2 + \dots + \tau_\alpha$. Similarly, computations resulting from multiple LTE eNBs at a single node can be aggregated and abstracted to a single τ_L . The proposed approach can be readily extended to more than two technologies that conduct their FFT computations by sharing the remote node.

E. Transport Protocols

A protocol is required to coordinate the I/Q data transmissions over the transport network. The strict latency requirements for the CRAN and DCCAP architectures limit the choice of generic protocols over Ethernet. Some of the fronthaul protocols that could be employed for the transport of information between headend/cloud and remote node are:

1) *Radio over Fiber (RoF)*: Radio over fiber (RoF) transports the radio frequency signal over an optical fiber link

by converting the electrically modulated signal to an optical signal [90]–[92]. RoF signals are not converted in frequency but superimposed onto optical signals to achieve the benefits of optical transmissions, such as reduced sensitivity to noise and interference. The remote nodes directly convert the optical signal to an electrical signal with minimal processing, reducing the cost of the remote node. However, the analog optical signal transmission in RoF suffers from more attenuation as compared to the transmission of digital data over the fiber.

We briefly note that so-called Radio-and-Fiber (R&F) networks are an alternative form of converged radio and fiber networks [93]–[95]. R&F networks typically consist of distinct wireless and optical network segments that each conduct their own specific physical and medium access control layer processing [94], [96], [97]. That is, R&F networks are typically deployed as two-level architectures with protocol translation at the interface between the radio and optical network segments. For CRAN architectures, the RoF transport is generally preferred over R&F networks as the RoF transport better supports centralized signal processing at the BBU [95]. The proposed R-FFT approach follows the generally strategy of the CRAN architecture to centralize signal processing at the BBU and therefore RoF transport appears better suited than R&F networking for the R-FFT approach.

2) *Common Public Radio Interface (CPRI)*: The eCPRI v1.0 specification [98]–[100] defines a generic protocol framework for transporting the I/Q symbols between the Remote Radio Unit (RRU) and the Base Band Unit (BBU) over a conventional transport network, such as Ethernet and optical transport networks. The eCPRI framework has been fundamentally defined to support a wide range of functional split options between RRU and BBU with variable transport bit rates. Our proposed R-FFT node corresponds to the low PHY functional split option as defined in the eCPRI specification. The eCPRI protocol framework is thus well suited as transport protocol between R-FFT node and Headend/BBU.

3) *Open Base Station Architecture Initiative (OBSAI)*: The Open Base Station Architecture Initiative (OBSAI) [101] is similar to CPRI in that the digitized time domain I/Q samples are transported over a fronthaul interface. The OBSAI would need to be adapted for the frequency I/Q transport. In contrast to CPRI, the OBSAI interface is an IP based connection. The IP logical connection can be implemented over any generic Ethernet link, providing flexible connectivity between headend/cloud and remote node.

a) *External PHY Interfaces*: The Downstream External PHY Interface (DEPI) [102] and Upstream External PHY Interface (UEPI) [103] enable the common transport mechanisms between an RPD and the CCAP core. DEPI and UEPI are based on the Layer 2 Tunneling Protocol version 3 (L2TPv3). The L2TPv3 transparently transports the Layer 2 protocols over a Layer 3 network by creating pseudowires (logical connections).

We note that the transport between R-FFT remote node and BBU needs to also comply with the delay requirements due to the hybrid automatic repeat request (HARQ) protocols operating in CRANs. The HARQ protocols impose latency requirements that in turn limit the distance between RRU and

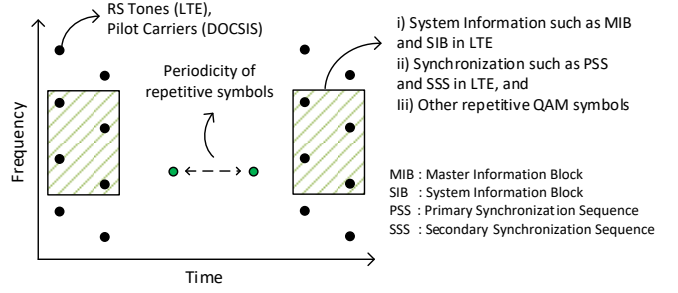


Fig. 7. Some QAM symbols pertaining to an OFDM symbol remain constant over time. For example, Reference Signal (RS) tones in LTE occur typically every four OFDM symbols; similarly, DOCSIS pilot tones repeat periodically. This periodically repeated QAM symbol information can be cached at the remote node to reduce the data rate over the digital Ethernet fiber link between the headend and the R-FFT node.

BBU, for example [24], [104]–[106] consider a 20–40 km RRU-BBU distance. These delay constraints for CRAN networks apply similarly to the R-FFT network. Fundamentally, the R-FFT node only reduces the fronthaul transmission bit rates and does not alter the delay requirements of the I/Q transport between BBU and RRH. Therefore, all the CRAN constraints and requirements for the delay apply analogously to the R-FFT network. On the other hand, the integration of the cable access network with the CRAN does not impose any additional delay requirements (in addition to the existing CRAN delay requirements) as there are no HARQ processes in the cable network. Thus, the LTE CRAN requirements dictate the delay limits for the combined deployments of CRAN and cable access networks in the proposed R-FFT architecture.

IV. PROPOSED REMOTE CACHING OF QAM SYMBOLS

In order to further reduce the bandwidth in addition to the function split process, several techniques, such as I/Q compression [9], [10], [12], [107], can be employed. In contrast, we propose OFDM resource element (time and frequency slot) allocation based remote caching. If some part of the information is regularly and repeatedly sent over the interface, a higher (orchestration, in case of SDN) level of the signaling process can coordinate caching mechanisms. For example, there is no need to transmit the downstream I/Q samples of the pilot tones as they remain constant in DOCSIS. Figure 7 gives an overview of repetitive QAM symbols in LTE and DOCSIS. The stationary resource elements across the time domain, such as the system information block (SIB), typically change over long time scales on the order of hours and days. The cached elements can be refreshed or re-cached through cache management and signalling protocols, see Sec. IV-D.

In contrast to the downstream, upstream information must be entirely transported to the headend to process all the signal components received by the R-FFT receiver.

In the evaluations of the overhead due to repetitive QAM symbols that can be saved through caching in this section, we evaluate the ratios (percentages) of number of repetitive I/Q symbols to total number of I/Q symbols. Subsequently, in the evaluations in Section V we evaluate the corresponding reductions of the fronthaul transmission bitrate.

A. LTE Networks

1) *Reference Signal (RS) Tones Caching*: RS tones are pilot subcarriers that are embedded throughout the operational wireless system bandwidth for channel estimation so as to equalize the impairments of the received wireless signal. More specifically, the RS tones consist of data that is known to both the wireless transmitter and receiver, whereby in the downstream direction the LTE eNB (RRU) co-located with the R-FFT node is the wireless transmitter and the UEs are the wireless receivers. The known RS tone data helps the wireless receivers (UEs) to determine the downlink power levels (of the signal arriving from the eNB) as well as to determine the channel characteristics (distortions) by comparing the received RS tone signals with the known RS tone data. Importantly, for a given cell deployment, the same RS tones are always transmitted at a constant power level by the eNB to the UEs so as to facilitate the estimation of the received power level and distortion after the signal propagation over the wireless channel between eNB and UEs. Thus, at the wireless transmitter (eNB) side, the transmitted RS tones are constant for a given cell deployment. Signal disturbances on the wireless channels are substantially more pronounced compared to signal propagation in wired channels. Therefore RS tones are added in close proximity with each other in LTE to accurately estimate the channel characteristics, such as coherence-time and coherence-bandwidth. The values and positions of the RS tones are fixed for a given deployment, i.e., the RS tones and the corresponding I/Q sample values do not change over time for a given wireless cell deployment. In particular, in LTE, as defined in the 3GPP specification TS 36.211 [108], the configuration of the cell-specific RS tones depends on the cell identity (ID) of the deployment, which is an integer value between 0 and 503. The cell ID is constant for a given physical deployment; hence, the RS tone configuration is also constant. Therefore, the RS tone caching at the R-FFT node has to be performed only once during the initialization and there is no need for updating the cached RS (pilot) tone signals.

For a single antenna, the RS tones are typically spaced six subcarriers apart in frequency such that eight RS tones exist in a single subframe (which consists of 14 OFDM symbols in the time dimension) and a single Resource Block (RB) (which consists of 12 LTE subcarriers in the frequency dimension). Thus, with a full RB allocation, i.e., for a relative payload data traffic load (intensity) of $\rho_L = 1$, approximately $8/(12 \times 14) = 4.7\%$ of I/Q transmissions over the digital fiber can be saved by caching RS tones at the remote node, regardless of the system bandwidth. In general, for a traffic intensity ρ_L , $\rho_L \leq 1$, the overhead due to RS tones in the LTE resource grid is

$$\text{RS Overhead} = \frac{8}{\rho_L \times 12 \times 14} = \frac{4.7}{\rho_L} \%. \quad (4)$$

When the user data traffic is very low, e.g., $\rho_L = 0.1$, the overhead is almost 47%, and similarly when $\rho_L = 0.01$ the overhead becomes 470%.

2) *PHY Broadcast Channel (PBCH) Caching*: The PHY Broadcast Channel (PBCH) carries the Master Information

Block (MIB) which is broadcast continuously by the eNB regardless of the user connectivity. The MIB includes basic information about the LTE system, such as the system bandwidth and control information specific to the LTE channel. The PBCH/MIB always uses the six central RBs (i.e., 72 subcarriers) for the duration of 4 OFDM symbols to broadcast the MIB data. The PBCH space in the resource grid is inclusive of the RS tones used in the calculation of Eqn. (4); therefore, the RS tones need to be subtracted when calculating the MIB overhead. The PBCH/MIB occurs once every 40 ms and there exist four redundant MIB versions. Once all the four versions are cached, the I/Q samples corresponding to the MIB PDU remain constant for the deployment and no further updates are required. The four redundant MIB versions are broadcast with an offset of 10 ms. Thus, an PBCH/MIB occurs effectively once in every 10 ms (radio frame). The PBCH/MIB overhead for an entire 20 MHz system LTE system with 1200 subcarriers, 14 OFDM symbols, and 10 subframes is thus

$$\text{PBCH Overhead} = \frac{6 \times 12 \times 4 - (8 \times 6)}{\rho_L \times 1200 \times 14 \times 10} = \frac{0.142}{\rho_L} \%. \quad (5)$$

Alternatively, for a 1.4 MHz system with 72 subcarriers (the lowest currently standardized LTE bandwidth, which would be used for IoT type of applications), the overhead increases to

$$\text{PBCH Overhead}_{1.4\text{MHz}} = \frac{6 \times 12 \times 4 - (8 \times 6)}{\rho_L \times 72 \times 14 \times 10} = \frac{2.3}{\rho_L} \%. \quad (6)$$

Future IoT related standardization efforts may lower the LTE rates below 1.4 MHz to better suit the needs of low-rate IoT applications, leading to further increases of the PBCH overhead.

3) *Synchronization Channel Caching*: The Synchronization Channel (SCH) consists of the Primary Synchronization Sequence (PSS) and the Secondary Synchronization Sequence (SSS), which are broadcast continuously by the eNB, regardless of the user connectivity. The PSS and SSS help with the cell synchronization of wireless users by identifying the physical cell ID and the frame boundaries of the LTE resource grid. Similar to the RS tones in Section IV-A1, the PSS and the SSS, i.e., the cell ID and frame boundary information, are static for a given cell deployment. Thus, caching the PSS and SSS does not degrade the functioning of the LTE cell. The PSS/SSS occurs every 5 ms (twice per radio frame) and uses six central RBs over two OFDM symbols. Similar to Eqns. (5) and (6), the overhead due to the PSS/SSS in 20 MHz and 1.4 MHz systems are

$$\begin{aligned} \text{SCH Overhead} &= \frac{6 \times 12 \times 4}{\rho_L \times 1200 \times 14 \times 10} = \frac{0.171}{\rho_L} \%. \\ \text{SCH Overh.}_{1.4\text{MHz}} &= \frac{6 \times 12 \times 4}{\rho_L \times 72 \times 14 \times 10} = \frac{2.8}{\rho_L} \%. \end{aligned} \quad (7)$$

4) *System Information Block (SIB) Caching*: In a similar way, the caching mechanism can be extended to the System Information Blocks (SIBs) broadcast messages of the LTE PHY Downlink Shared Channel (PDSCH). There are 13 different SIB types, ranging from SIB1 to SIB13. SIB1 and SIB2 are mandatory broadcast messages that are mostly static for a given cell deployment. More specifically, SIB1 contains

a System Information info-tag bit. This info-tag bit changes when the deployment characteristics change, e.g., when a new neighbor cell is added or a new feature is added to the existing cell. Such changes typically occur only every few weeks or months. When such a change happens, then the info-tag bit signals that all SIBs need to be updated. Similarly, the other SIBs depend on the relations between the serving cell and the neighbor cell configurations. In a typical deployment, SIB3 to SIB9 are manually configured and can be combined in a single message block for the resource block allocation. Typical RB allocation configurations schedule the SIB1 and SIB2 transmissions over 8 RBs across 14 OFDM symbols in time (i.e., 1 subframe), with an effective periodicity (with redundant version transmissions) of 2 radio frames (i.e., 20 ms). The overhead from the SIB1 and SIB2 transmissions while subtracting the corresponding RS tones overhead of 8×8 , i.e., 8 tones per RB for 8 RBs, is

$$\begin{aligned} \text{SIB Overhead} &= \frac{8 \times 12 \times 14 - (8 \times 8)}{\rho_L \times 1200 \times 14 \times 20} = \frac{0.381}{\rho_L} \% \\ \text{SIB Overh.}_{1.4\text{MHz}} &= \frac{8 \times 12 \times 14 - (8 \times 8)}{\rho_L \times 72 \times 14 \times 20} = \frac{6.3}{\rho_L} \% \end{aligned} \quad (8)$$

The resource allocation and periodicity of the higher order SIBs, i.e., from SIB3 to SIB9, can vary widely and it is therefore difficult to accurately estimate the overhead. We consider therefore only the SIB1 and SIB2 caching in our evaluation of the cache savings. However, a signalling and cache management protocol, as outlined in Section IV-D, can coordinate the caching of the higher order SIBs and thus achieve further savings.

B. Cable Networks

In DOCSIS 3.1, downstream pilot subcarriers are modulated by the CMTS with a predefined modulation pattern which is known to all CMs to allow for interoperability. Two types of pilot patterns are defined in DOCSIS 3.1 for OFDM time frequency grid allocations: i) continuous, and ii) scattered. In the continuous pilot pattern, pilot tones with a predefined modulation occur at fixed frequencies in every symbol across time. In the scattered pilot pattern, the pilot tones are swept to occur at each frequency locations, but at different symbols across time. The scattered pilot pattern has a periodicity of 128 OFDM symbols along the time dimension such that the pattern repeats in the next cycle. Scattered pilots assist in the channel estimation. Typical deployments have 192 MHz operational bandwidth [109], corresponding to an FFT size of 8192 with 25 kHz subcarrier spacing. A 192 MHz system has 7680 subcarriers, including 80 guard band subcarriers, 88 continuous pilot subcarriers, and 60 scattered pilot subcarriers. Therefore, the overhead due to guard band and pilot subcarriers, which can be cached at the remote node, is

$$\text{Cable Over.} = \frac{80 + 88 + 60}{\rho_C \times 7680} = \frac{2.9}{\rho_C} \% \quad (9)$$

C. Memory Requirements for Caching

The caching of frequency domain OFDM I/Q symbols requires caching memory at the remote node. Each I/Q symbol

that needs to be cached is a complex number with real and imaginary part. For the purpose of evaluation, we follow [8], [36] and consider a 10 bit representation for each part of the complex number, resulting in a 20 bit memory requirement for each frequency domain QAM symbol. A 30 bit representation of a frequency domain QAM symbol, as considered in [98], would correspondingly increase the memory requirements. The caching of LTE RS tones saves 4.7 % of the fronthaul transmissions as shows in Eqn. (4). Within each RB, 8 RS tones exist for every 12 subcarriers. A typical 20 MHz system with 1200 subcarriers, has thus 8×100 RS tones. The total memory required to cache the RS tones QAM symbol data is

$$\text{RS Tones Mem.} = (8 \times 100) \times 2 \cdot 10 \text{ bits} = 16000 \text{ bits.} \quad (10)$$

Similarly, caching of the PBCH, SCH, and SIB data requires

$$\begin{aligned} \text{PBCH Mem.} &= (6 \times 12 \times 4 - (8 \times 6)) \times 2 \cdot 10 \text{ bits} \\ &= 4800 \text{ bits,} \end{aligned} \quad (11)$$

$$\text{SCH Mem.} = (6 \times 12 \times 4) \times 2 \cdot 10 = 5760 \text{ bits,} \quad (12)$$

$$\begin{aligned} \text{SIB Mem.} &= (8 \times 12 \times 14 - (8 \times 8)) \times 2 \cdot 10 \text{ bits} \\ &= 5760 \text{ bits.} \end{aligned} \quad (13)$$

For DOCSIS, the cache memory requirement for the continuous and scattered pilots is

$$\text{Pilot Tones Mem.} = (80 + 88 + 60) \times 2 \cdot 10 \text{ bits} = 4560 \text{ bits.} \quad (14)$$

Thus, based on Eqns. (4)–(9), total savings of approx. 7 % to 18 % can be achieved in the fronthaul transmissions when the full resource allocation ($\rho = 1$) over the entire bandwidth is considered in both LTE and DOCSIS. For lower allocations, i.e., when there is less user data ($\rho < 1$), the caching can achieve much more pronounced fronthaul transmission bitrate reductions. In the extreme case, when there is no user data, all the cell specific broadcast data information can be cached at the remote node and the fronthaul transmissions can be completely suspended. The total memory for the caching required at the remote node based on Eqns. (10)–(14) is less than 37 kbits. The implementation of less than 5 kbytes cache memory at the remote node appears to be relatively simple and no significant burden for the existing remote nodes. Therefore, we believe that fronthaul transmission bitrate reductions of more than 7 % with almost negligible implementation burden is a significant benefit.

D. Signalling and Cache Management Protocol

The signalling and cache management protocol involves: i) transporting the caching information to the remote nodes, ii) updating the cached information at the remote nodes with new information, and iii) establishing the rules for reading cached resource elements at the remote node. Signalling protocol modules at the headend/cloud and remote node coordinate with each other through a separate (i.e., non-I/Q transport) logical connection between the headend/cloud and remote node, as summarized in Algorithm 1. Some of the cached information may change over time; however, these changes occur typically at much longer timescales compared to the I/Q

transmissions from the headend to the remote node. Due to the very long time scale of cache changes, i.e., very infrequent cache changes, the signalling overhead which arises from the cache management is typically negligible. The reading (retrieval) of the cached content has to be precisely executed with accurate insertion of the subcarrier information in the particular time and frequency locations.

V. PERFORMANCE EVALUATION

A. Reduction of Downstream Fronthaul Bitrates due to Caching

Tables II and III compare the downstream fronthaul transmission bitrate requirements for I/Q transmissions in an FFT-split system without and with caching of the repetitive I/Q QAM symbols for different packet traffic payloads (intensities) ρ_L and ρ_C and code rates of 0.9, 0.7, and 0.5, for the LTE and DOCSIS systems, respectively. Tables II and III also report the corresponding transmission bitrate reductions (in percent) achieved by caching the repetitive I/Q QAM symbols. Based on the evaluations in Sec. IV, we consider an I/Q QAM symbol overhead of 7 % in LTE, including RS tones, PBCH, PSS/SSS, and SIB, for a system with a bandwidth somewhat below 20 MHz. For DOCSIS we consider a 3 % overhead due to continuous and scattered pilots, approximating the 2.9 % found in Eqn. (9). The actual payload traffic rates are based on wireless and cable link capacities of $R_L = R_C = 1$ Gbps, e.g., for the traffic intensity $\rho_L = 0.01$, the actual LTE payload traffic rate is $\rho_L \times R_L = 10$ Mbps. The fronthaul I/Q data rate originating from the payload traffic depends on the QAM size and code rate of the system. With $K = 10$ bits required to represent each complex and real part of a QAM I/Q symbol, the fronthaul transmission bitrate required for the payload data can be evaluated as

$$R_{\rho, \text{Payload}}^F = \frac{\rho \times R}{\text{Code Rate} \times \text{QAM Size}} \times 2 \cdot K. \quad (15)$$

And the excess I/Q transmission bitrate required due to the overhead (non-payload) can be evaluated as

$$R_{\rho, \text{Overhead}}^F = \text{Overhead Percentage} \times R_{\rho=1, \text{Payload}}^F. \quad (16)$$

The total required fronthaul transmission bitrate is the sum of bitrates arising from overhead and payload I/Q transmissions, i.e.,

$$R_{\rho, \text{Total}}^F = R_{\rho, \text{Payload}}^F + R_{\rho, \text{Overhead}}^F. \quad (17)$$

Note that the system bandwidth R_F from Eqn. (3) provided by the employed subcarriers must be high enough to accommodate the fronthaul transmission bitrate $R_{\rho, \text{Total}}^F$ arising from the payload traffic intensity ρ , i.e., $R_{\rho, \text{Total}}^F \leq R_F$.

From Table II, we observe that the reductions of the total I/Q fronthaul data rates with caching are proportionally higher for lower offered loads ρ_L . This is because the overhead data rate $R_{\rho, \text{Overhead}}^F$ is fixed at a value corresponding to the fully loaded ($\rho_L = 1$) LTE system, whereas the I/Q payload bitrate varies with the actual payload. Caching eliminates the overhead rate $R_{\rho, \text{Overhead}}^F$ and thus reduces the total fronthaul bitrates. For example, for the code rate = 0.9, for $\rho_L = 0.01$, the total data rate without caching is 0.296 Gbps, which is nearly 30 times

of the offered load $\rho_L R_L$; when $\rho_L = 1$, the total fronthaul data rate without caching is 3.962 Gbps, which is nearly four times of the offered load $\rho_L R_L$. However, when caching is employed, for both loads $\rho_L = 0.01$ and 1, the total data rates are 3.7 and 3.33 times of the offered load, respectively. Higher bitrate savings can be achieved at lower loads as compared to higher loads. For $\rho_L = 0.01$, the total savings is 87.50 %, compared to 6.54 % savings for $\rho_L = 1$.

For both data rates, with and without caching, we observe linear increases with decreasing code rates. For example, for $\rho_L = 0.01$, the data rate without caching is increased from 0.296 Gbps for the code rate 0.9 to 0.380 Gbps for the code rate 0.7, i.e., the data rate is increased by a factor of $0.9/0.7 = 1.27$. Since both the data rate with caching and the data rate without caching scale linearly by a constant factor with the decreasing code rate, the bitrate savings achieved from the overhead caching is independent of the code rates. However, the choice of code rate for fronthaul I/Q generation significantly affects the total data rates. Higher code rates reduce the fronthaul requirements by lowering the total data rate.

The throughput requirements for the DOCSIS fronthaul I/Q transmissions presented in Table III show similar behaviors as the LTE results presented in Table II. However, as compared to the LTE fronthaul I/Q requirements for the same link capacity of $R_C = R_L = 1$ Gbps, the DOCSIS protocol requires relatively lower bitrates. This is because, the DOCSIS protocol supports a higher QAM size of 4096 (2^{12}) than LTE; thus DOCSIS transports more bits per I/Q symbol transmission. The DOCSIS overhead percentage arising from the continuous and scattered pilot, which can be cached at the remote node, is 3 %. Therefore, the effective savings in DOCSIS are relatively smaller compared to LTE. Nevertheless, the fronthaul bitrate savings are 2.9 % for a fully loaded ($\rho_C = 1$) DOCSIS system and 23 % for a 10 % ($\rho_C = 0.1$) loaded system.

B. Total LTE + Cable Fronthaul Bitrate for Different Function Splits

The downstream fronthaul transmission bitrate requirements to concurrently support LTE and DOCSIS deployments over a shared optical infrastructure are shown in Table IV. The FFT split, baseband, and passband fronthaul bitrates are evaluated based on Eqns. (15)–(17) and (1)–(3). For the purpose of the evaluation, we consider $W = 1$ antenna, a code rate (CR) of 0.9, carrier frequencies of $f_c = 2$ GHz and 1 GHz, sampling frequencies of $f_s = 30.72$ MHz and 204.8 MHz, symbol durations of $T = 66.7 \mu\text{s}$ and $20 \mu\text{s}$, link capacities of $R = 1$ Gbps, and cached overhead of 7 % and 3 % for LTE and DOCSIS, respectively. We observe from Table IV that the bitrates decrease as the position of the function split is moved from passband (i.e., remote DAC/ADC) to remote-PHY (i.e., from right to left in Fig. 4).

The passband bitrates $R_{\text{LTE}}^P = 40$ Gbps [Eqn. (1) evaluated with $f_c = 2$ GHz] and $R_{\text{DOC}}^P = 20$ Gbps [Eqn. (1) evaluated with $f_c = 1$ GHz] are independent of the offered payloads ρ_L and ρ_C . Similarly, the baseband bitrates $R_{\text{LTE}, 20 \text{ MHz}}^B = 1.23$ Gbps [Eqn. (2) evaluated with $f_s =$

TABLE II

DOWNSTREAM LTE FRONTHAUL BITRATES WITHOUT CACHING [$R_{\rho, \text{TOTAL}}^F$, EQN. (15)] AND WITH CACHING [$R_{\rho, \text{PAYLOAD}}^F$, EQN. (17)], AS WELL AS BITRATE REDUCTIONS DUE TO I/Q CACHING WITH 7% OVERHEAD IN FFT-SPLIT LTE SYSTEM WITH QAM SIZE 64 (2^6), FOR DIFFERENT PAYLOADS ρ_L AND CODE RATES 0.9, 0.5, AND 0.7.

| LTE Load ρ_L | LTE FFT-Split Fronthaul I/Q Data Rate (Gbps) | | | | | | % Sav. |
|-------------------|--|----------|----------------|----------|----------------|----------|--------|
| | Code Rate= 0.9 | | Code Rate= 0.7 | | Code Rate= 0.5 | | |
| | w/o cach. | w/ cach. | w/o cach. | w/ cach. | w/o cach. | w/ cach. | |
| 0.01 | 0.296 | 0.037 | 0.380 | 0.047 | 0.533 | 0.066 | 87.50 |
| 0.1 | 0.629 | 0.370 | 0.809 | 0.476 | 1.133 | 0.666 | 41.17 |
| 0.2 | 1.000 | 0.740 | 1.285 | 0.952 | 1.800 | 1.333 | 25.92 |
| 1 | 3.962 | 3.333 | 5.095 | 4.761 | 7.133 | 6.666 | 6.54 |

TABLE III

DOWNSTREAM CABLE FRONTHAUL BITRATES WITHOUT CACHING ($R_{\rho, \text{TOTAL}}^F$) AND WITH CACHING ($R_{\rho, \text{PAYLOAD}}^F$), AND BITRATE REDUCTIONS DUE TO I/Q CACHING WITH 3% OVERHEAD IN FFT-SPLIT DOCSIS SYSTEM WITH QAM SIZE 4096 (2^{12}), FOR DIFFERENT PACKET PAYLOADS ρ_C AND CODE RATES 0.9, 0.5, AND 0.7

| DOCSIS Load ρ_C | DOCSIS FFT-Split Fronthaul I/Q Data Rate (Gbps) | | | | | | % Sav. |
|----------------------|---|----------|----------------|----------|----------------|----------|--------|
| | Code Rate= 0.9 | | Code Rate= 0.7 | | Code Rate= 0.5 | | |
| | w/o cach. | w/ cach. | w/o cach. | w/ cach. | w/o cach. | w/ cach. | |
| 0.01 | 0.074 | 0.018 | 0.095 | 0.023 | 0.133 | 0.033 | 75.00 |
| 0.1 | 0.240 | 0.185 | 0.309 | 0.238 | 0.433 | 0.333 | 23.07 |
| 0.2 | 0.425 | 0.370 | 0.547 | 0.476 | 0.766 | 0.666 | 13.04 |
| 1 | 1.907 | 1.851 | 2.452 | 2.380 | 3.433 | 3.333 | 2.91 |

TABLE IV

TOTAL DOWNSTREAM LTE + CABLE FRONTHAUL BITRATES FOR DIFFERENT SPLITS: PHY (ENTIRE PHY PROCESSING AT REMOTE NODE), R-FFT (PROPOSED, WITH AND WITHOUT CACHING FOR CODING RATIO 0.9), BASEBAND (CONVENTIONAL CRAN), AND PASSBAND SPLIT FOR RANGE OF LTE AND DOCSIS PAYLOAD TRAFFIC INTENSITY LEVELS ρ_L AND ρ_C FOR LTE AND DOCSIS CAPACITIES $R_L = R_C = 1$ Gbps.

| Fronthaul Traffic (Gbps) | | | | | | | | | | | | | |
|---|---------------------|--|-------|-------|-----------------------|-------|-------|---------------------------------|-------|--------|---------------------------------|------|-------|
| PHY Split, payload intensity (ρ), payload bitrates $\rho_L R_L$ and $\rho_C R_C$ | | FFT split R_{ρ}^F , Eqns. (15) and (17) | | | | | | Baseband split R^B , Eqn. (2) | | | Passband split R^P , Eqn. (1) | | |
| | | w/ caching (CR= 0.9) | | | w/o caching (CR= 0.9) | | | | | | | | |
| LTE (ρ_L) | DOCSIS (ρ_C) | LTE | DOC. | Total | LTE | DOC. | Total | LTE | DOC. | Total | LTE | DOC. | Total |
| 0.01 | 0.01 | 0.037 | 0.018 | 0.055 | 0.296 | 0.074 | 0.370 | 18.45 | 8.192 | 26.642 | 40 | 20 | 60 |
| 0.10 | 0.10 | 0.370 | 0.185 | 0.555 | 0.629 | 0.240 | 0.869 | | | | | | |
| 0.20 | 0.20 | 0.740 | 0.370 | 1.110 | 1.000 | 0.425 | 1.425 | | | | | | |
| 1.00 | 1.00 | 3.333 | 1.851 | 5.184 | 3.926 | 1.907 | 5.833 | | | | | | |

30.72 MHz] and $R_{\text{DOC}}^B = 8.19$ Gbps [Eqn. (2) evaluated with $f_s = 204.8$ MHz] for baseband I/Q time sample transport are independent of the offered payloads. The LTE baseband bitrate $R_{\text{LTE}, 20 \text{ MHz}}^B = 1.23$ Gbps is evaluated for a 20 MHz system, which can typically support payload bitrates up to around $R_L = 70$ Mbps with a single antenna. Therefore, to support the payload bit rate (capacity) of $R_L = 1$ Gbps, the LTE system needs to be scaled up by a factor of at least 15, e.g., to an LTE system with 2 antennas, 256 QAM, and 100 MHz bandwidth, which can support the 1 Gbps bitrate [110]. Thus, the effective LTE baseband bitrate to support 1 Gbps payload is $15 \cdot R_{\text{LTE}, 20 \text{ MHz}}^B = 15 \cdot 1.23 = 18.45$ Gbps. The FFT split fronthaul bitrates with and without caching are derived from Tables II and III. We observe from Table IV that for a system (without caching) loaded at 10 % ($\rho_L = \rho_C = 0.1$), the R-FFT approach reduces the fronthaul bitrate to 0.87 Gbps compared to 26.64 Gbps with the conventional baseband split; thus, the R-FFT approach reduces the fronthaul bitrate to one thirtieth compared to the conventional CRAN baseband split for this lightly loaded scenario. For a fully loaded ($\rho_L = \rho_C = 1$) system, R-FFT reduces the fronthaul bitrate to roughly one fifth of the baseband split.

C. Delay Evaluation

We proceed to illustrate the delay implications of the proposed R-FFT deployment in comparison to the existing R-PHY deployment. In particular, we consider transitioning a DOCSIS cable system from R-PHY to R-FFT operation, while sharing the fronthaul link with a fixed LTE CRAN deployment that transmits a prescribed traffic load (intensity) ρ_B (relative to the fronthaul transmission bitrate R_o) of baseband time domain I/Q sample data.

1) *Simulation Set-up*: We developed a simulation framework in the discrete event simulator OMNET++ to model the DCCAP cable architecture of the HFC network. A remote cable node, i.e., R-PHY or R-FFT node, is connected to the headend through an optical fiber with CIN distance d and transmission bitrate $R_o = 10$ Gbps. We vary the CIN distance d between 10 and 50 km to cover the distances of typical real deployment scenarios.

200 cable modems (CMs) are connected to the remote node through an analog broadcast cable. The distances from CMs to the remote node are uniformly distributed between 1 and 2 km in our simulations, and the CMs are polled in shortest propagation delay order [111]. Each CM has an infinite buffer in the simulation model and independently generates self-similar traffic with varying levels of burstiness characterized

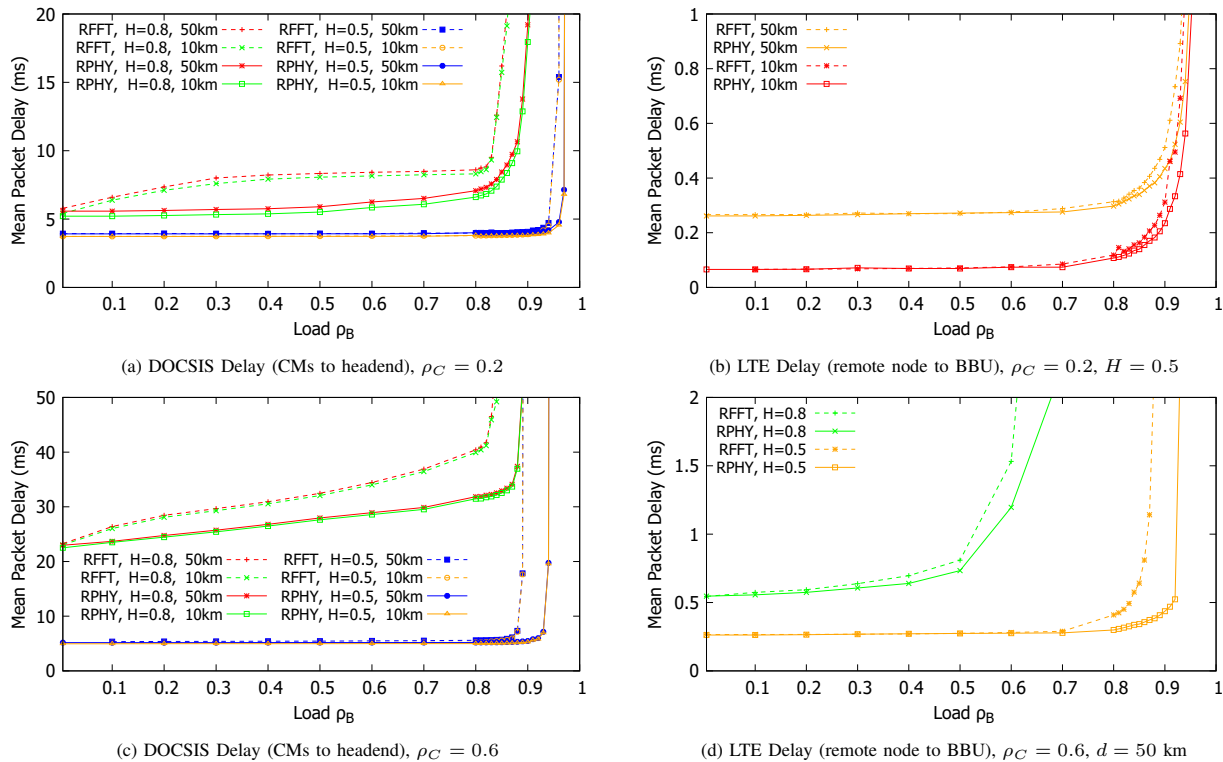


Fig. 8. Mean upstream DOCSIS and LTE packet delays for R-FFT and R-PHY cable system supporting a prescribed load ρ_B of baseband LTE traffic.

by the Hurst parameter H with an average packet size of 472 byte. The Hurst parameter $H = 0.5$ corresponds to Poisson traffic, and the burstiness increases for increasing H . We consider $H = 0.8$ as typical Hurst parameter for self-similar traffic in our simulations. The DOCSIS 3.1 protocol coordinates the cable transmissions in the broadcast cable with the transmission bitrate $R_C = 1$ Gbps in each direction. Throughout, we assume that 20 % of the cable transmission bit rate R_C is occupied with contention and maintenance slots. Thus, only 80 % of the cable transmission bit rate R_C are available for data transmissions. The Double Phase Polling (DPP) protocol [112]–[114] controls the upstream transmissions of the 200 distributed CMs over the shared broadcast cable. For R-PHY, DOCSIS PHY frames are digitized and transported over the Upstream External PHY Interface (UEPI) with prioritized CIN transmission of the upstream transmission requests. For R-FFT operation, the upstream cable data is converted to frequency I/Q symbols and transported in generic UDP packets. An FFT size of 4096, which corresponds to $T_C = 40 \mu s$, and QAM size of 12 bits with code rate 0.9 are used for converting the upstream data to frequency domain I/Q symbols. Each complex number representing an I/Q symbol is digitized with $2 \cdot K = 20$ bits.

We consider the deployment of an LTE RRU at the remote cable node (R-FFT or R-PHY). The LTE RRU implements the conventional LTE CRAN baseband function split, i.e., injects the baseband time domain I/Q samples with bitrate $\rho_B R_o$ into the cable remote node. The LTE upstream traffic and the cable upstream traffic share the optical transmission bitrate R_o from the remote node to the headend, where the BBU CRAN and the cable headend are implemented. We model a typical FIFO

queue at the remote node to forward the LTE packets to the CRAN BBU.

The average mean packet delays were sampled from over 600 s of simulated network operation, with an additional 10 s of warm-up before collecting samples, for each given simulation scenario. Thus, over 180 Million packets were sampled for each considered simulation scenario. We verified that the 98 % confidence intervals resulting from 10 Million simulated Poisson traffic packets were well below 2 % of the corresponding sample means. We do not plot the confidence intervals as they would not be visible. The over 180 Million simulated packets for each scenario result in consistent reliable mean packet delay estimates, as demonstrated by the smooth curves in Fig. 8.

2) *DOCSIS Delay*: Figure 8 compares the mean upstream DOCSIS and LTE packet delays when the cable remote node is operated as either R-FFT or R-PHY node. Figs. 8(a) and (c) show the mean cable (DOCSIS) upstream packet delay from the CMs to the headend as a function of LTE fronthaul traffic intensity ρ_B , which corresponds to the LTE I/Q sample bitrate $R^B = \rho_B R_o$ for different optical distances d and traffic burstiness levels H . The cable traffic intensity is fixed at $\rho_C = 0.2$, which corresponds to the cable traffic rate $\rho_C R_C = 0.2 \times 1 \text{ Gbps} = 200 \text{ Mbps}$.

From Figs 8(a) and (c) we observe that the transition from operating the cable remote node as R-PHY node to R-FFT node slightly increases the mean DOCSIS packet delays for the bursty $H = 0.8$ traffic, whereas the mean DOCSIS packet delays are not visibly increased for Poisson LTE traffic loads below $\rho_B = 0.88$. However, for very high ρ_B loads, the R-FFT DOCSIS delays shoot up to very high values at

lower ρ_B Poisson loads than the R-PHY DOCSIS delays. The underlying cause for these observations is the increase of the cable bitrate due to the processes of I/Q conversion and digitization. For the 9/10 code rate, 12 bits QAM size, and $2 \cdot K$ bits for representing the real and imaginary parts of the I/Q samples, the cable bitrate is increased by a factor of $(10/9) \times (1/12) \times 2 \cdot 10 = 1.85$ [see Eqn. (15)]. There is some overhead in the uplink, e.g., for uplink pilot tones; however, there is no overhead due to broadcast of PHY layer attributes, such as MIB, SIB and PSS/SSS, in the uplink. We neglect therefore the uplink overhead, which is low compared to the 1.85 fold bitrate increase due to the I/Q conversion and digitization, in the uplink delay evaluation.

This 1.85 fold increase of the cable traffic portion on the fronthaul link results in negligible mean delay increases for low to moderate Poisson traffic loads. However, for high Poisson traffic loads, the increased cable traffic portion reduces the LTE bitrate ρ_B up to which low DOCSIS delays are achieved. In particular, for $\rho_C = 0.6$ considered in Fig. 8(c), the cable bitrate is increased from $\rho_C R_C = 600$ Mbps for R-PHY to $1.85 \cdot 600$ Mbps ≈ 1.1 Gbps; accordingly, the tolerable LTE traffic load is reduced from close to $R_o - 600$ Mbps = 9.6 Gbps, i.e., $\rho_B = 0.96$, for cable R-PHY operation to only close to $\rho_B = 0.89$ for cable R-FFT operation. Similarly, for bursty self-similar traffic with $H = 0.8$, the increase of the cable traffic portion with R-FFT leads to more frequent temporary spikes of the total LTE plus cable bitrate above the R_o fronthaul link capacity, increasing the mean DOCSIS packet delay compared to cable R-PHY operation.

3) *LTE Delay*: Fig. 8(b) shows the mean LTE fronthaul packet delay for R-FFT and R-PHY operation of the cable remote node for different optical fronthaul distances of $d = 10$ and 50 km. We observe from Fig. 8(b) that the longer 50 km fronthaul distance increases the LTE packet delay compared to the 10 km distance due to the propagation delay increase [of $40 \text{ km}/(2 \cdot 10^8 \text{ m/s})$] on the optical fiber. We also observe that the R-FFT cable node operation supports very slightly lower LTE traffic loads ρ_B due to the increase of the cable traffic portion from the I/Q conversion and digitization. Fig. 8(d) shows the mean LTE packet delay as a function of the LTE fronthaul bitrate ρ_B for Poisson ($H = 0.5$) and bursty ($H = 0.8$) traffic. We observe that the bursty traffic results generally in higher LTE mean packet delays and gives rise to pronounced delay increases for LTE traffic loads ρ_B exceeding 0.5.

Overall, the evaluations in Figs. 8(b) and (d) indicate that for low to moderately high traffic loads, the LTE traffic suffers less than 1 ms delay. We note that according to the LTE protocol specifications, the LTE protocol operation is tightly coupled to a synchronous timeline. In particular, the LTE protocol operates based on 1 ms sub-frames. The end-to-end network delay along with the processing delay is accommodated by a 4 ms separation between an uplink request and the corresponding downlink transmission. Thus, in the R-FFT implementation, the total delay (network and processing), including the jitter variations of I/Q data between BBU and the R-FFT node, can typically be readily accommodated within the uplink-downlink time separation on the operational timeline of the LTE protocol.

We note that the delay evaluations in this section considered the transition of the cable remote node from R-PHY to R-FFT operation while keeping the LTE CRAN operation unchanged. In particular, the cable traffic bitrate increased from the PHY payload $\rho_C R_C$ to the FFT split bitrate [which corresponds to $R_{\rho, \text{Payload}}^F$, Eqn. (15)], while the LTE traffic bitrate stayed unchanged at the baseband split rate R^B [Eqn. (2)]. The presented delay results represent therefore a conservative assessment of the proposed R-FFT operation in that a consequent transition to R-FFT operation that includes the transition from the conventional CRAN baseband split to the proposed R-FFT split would reduce the LTE traffic portion. That is, the LTE traffic portion would be reduced from the baseband split bitrate R^B [Eqn. (2)] to the FFT split bitrate R^F [Eqns. (15)–(17), resp. Eqn. (3)], which is a substantial bitrate reduction. We also note that in such a consequent transition from the conventional R-PHY operation of the cable remote node and the CRAN (baseband split) operation of the LTE system to the proposed FFT split, the bitrate reduction of the LTE traffic (from baseband to FFT split) by far outweighs the cable traffic bitrate increase (from PHY split to FFT split). Thus, a consequent transition to the proposed FFT split will reduce the traffic bitrates on the fronthaul link and correspondingly reduce delays.

VI. CONCLUSIONS

We have developed a unified cable DOCSIS and wireless cellular LTE access network architecture with a novel Remote-FFT (R-FFT) node. The proposed R-FFT architecture supports both wired DOCSIS service to cable modems and cellular wireless LTE service over the installed hybrid fiber-broadcast cable infrastructure. More specifically, DOCSIS and LTE share the fronthaul fiber link from headend to R-FFT remote node as well as the IFFT/FFT module in the R-FFT node. The DOCSIS cable headend and LTE baseband unit send frequency domain I/Q symbols over the fronthaul fiber, reducing the bitrate compared to the conventional time domain I/Q symbol transmission. Also, the R-FFT node caches repetitive DOCSIS and LTE QAM symbols to further reduce the downstream bitrate requirements over the fiber link. Whereas conventional cloud radio access networks require the continuous transmission of time domain I/Q symbols over the fronthaul fiber, our R-FFT approach with caching can temporarily suspend or statistically multiplex the downstream transmission of frequency domain I/Q symbols if there is no downstream payload traffic. Our evaluations indicate that the bitrate savings achieved with QAM symbol caching increase substantially for low payload traffic levels. For typical DOCSIS scenarios, the caching savings increase from 2.9 % for a full DOCSIS load to 23 % caching savings with a 10 % cable traffic load. For LTE, the savings increase from 6.5 % for a full wireless traffic load to 41 % for a 10 % LTE traffic load.

Our evaluations also indicate that for a fully loaded system without caching, the R-FFT approach reduces the total fronthaul bitrate required for supporting cable and LTE wireless service to roughly one fifth of the bitrate for the conventional baseband approach of transmitting time-domain

I/Q symbols. For 10 % cable and LTE traffic load levels, our R-FFT approach reduces the fronthaul bitrate in each direction (upstream and downstream) to approximately 1/30 of the conventional baseband approach. We have also demonstrated that transitioning a conventional R-PHY cable remote node to an R-FFT remote node (while keeping the LTE baseband operation unchanged) incurs only minute delay increases. The transition to cable R-FFT allows for the flexible efficient execution of all physical layer processing steps (except the FFT, DAC, and upconversion) in software on generic computing hardware at the headend, reducing the cost and complexity of the remote node.

We note that the proposed R-FFT network approach aligns closely with the main 5G technology development trends [115]–[118]. One main trend in 5G technology development and deployment, especially in the fronthaul, backhaul, and core networks, is to unify the heterogeneous access networks. Our R-FFT approach to integrate the cable and traditional cellular networking in the access domain is consistent with the 5G principles of unifying the heterogeneous access networks. Another important aspect of 5G is softwarization of traditional network applications, such as policy enforcement and virtualization of network functions, e.g., packet gateway functions. Towards this end, the primary goals of the CRAN and CCAP architectures are to softwarize and virtualize functions of cellular and cable networks. Thus, our proposed R-FFT architecture is overall closely aligned with the main directions of 5G technology progress and deployment.

There are several exciting directions for future research on unifying broadcast cable and cellular wireless access. One particularly important direction is to investigate how Internet of Things (IoT) applications and traffic flows, which consist typically of small intermittently transmitted data sets, can be efficiently served. Future research should investigate the quality of service and quality of experience achieved over the R-FFT network for IoT applications as well as a wide range of general applications that require access network transport. Additional caching mechanisms may be useful in efficiently serving very large numbers of such intermittent IoT flows. Another direction is to examine and improve the interactions of the R-FFT remote nodes and headends (BBUs) with the corresponding metropolitan area networks [119]–[123] and radio backhaul (core) networks [124]–[126]. Moreover, a prototype implementation of the R-FFT approach and evaluations through measurements in the prototype R-FFT network are an important directions for future work.

REFERENCES

- [1] CableLabs, “Data-over-cable service interface specifications DCA-MHAv2,” 2014.
- [2] Z. Alharbi, A. Thyagaturu, M. Reisslein, H. ElBakoury, and R. Zheng, “Performance comparison of R-PHY and R-MACPHY modular cable access network architectures,” *IEEE Transactions on Broadcasting*, in print, 2017.
- [3] J. Chapman, “Remote PHY for converged DOCSIS, Video, and OOB,” in *NCTA Spring Techn. Forum Proc.*, June 2014.
- [4] J. Chapman, G. White, and H. Jin, “Impact of CCAP to CM distance in a Remote PHY architecture,” in *INTX Spring Techn. Forum Proc.*, May 2015.
- [5] L. Dai, “An uplink capacity analysis of the distributed antenna system (DAS): From cellular DAS to DAS with virtual cells,” *IEEE Trans. on Wireless Commun.*, vol. 13, no. 5, pp. 2717–2731, May 2014.
- [6] A. Galis, S. Clayman, L. Mamatas, J. R. Loyola, A. Manzalini, S. Kuklinski, J. Serrat, and T. Zahariadis, “Softwarization of future networks and services-programmable enabled networks as next generation software defined networks,” in *Proc. IEEE Future Networks and Services*, 2013, pp. 1–7.
- [7] B. Hamzeh, M. Toy, Y. Fu, and J. Martin, “DOCSIS 3.1: Scaling broadband cable to gigabit speeds,” *IEEE Commun. Mag.*, vol. 53, no. 3, pp. 108–113, Mar 2015.
- [8] D. Wubben, P. Rost, J. Bartelt, M. Lalam, V. Savin, M. Gorgoglione, A. Dekorsy, and G. Fettweis, “Benefits and impact of cloud computing on 5G signal processing: Flexible centralization through cloud-RAN,” *IEEE Signal Proc. Mag.*, vol. 31, no. 6, pp. 35–44, Nov 2014.
- [9] K. F. Nieman and B. L. Evans, “Time-domain compression of complex-baseband LTE signals for cloud radio access networks,” in *Proc. IEEE Globecom*, 2013, pp. 1198–1201.
- [10] S. Nanba and A. Agata, “A new IQ data compression scheme for fronthaul link in centralized RAN,” in *Proc. IEEE PIMRC Workshops*, 2013, pp. 210–214.
- [11] B. Guo, W. Cao, A. Tao, and D. Samarzija, “LTE/LTE-A signal compression on the CPRI interface,” *Bell Labs Technical Journal*, vol. 18, no. 2, pp. 117–133, Sep. 2013.
- [12] —, “CPRI compression transport for LTE and LTE-A signal in C-RAN,” in *Proc. IEEE CHINACOM*, 2012, pp. 843–849.
- [13] S. Bhatia, R. Bartos, and C. Godsay, “Empirical evaluation of upstream throughput in a DOCSIS access network,” in *Proc. IEEE Int. Conf. on Multimedia Services Access Networks (MSAN)*, 2005, pp. 106–110.
- [14] S. Fulton, C. Godsay, and R. Bartoš, “DOCSIS as a foundation for residential and commercial community networking over hybrid fiber coax,” in *Broadband Services: Business Models and Technologies for Community Networks*, I. Chlamtac, A. Gumaste, and C. Szabo, Eds. Wiley, Hoboken, NJ, 2005, pp. 201–214.
- [15] C. Heyaime-Duvergé and V. K. Prabhu, “Statistical multiplexing of upstream transmissions in DOCSIS cable networks,” *IEEE Trans. Broadcasting*, vol. 56, no. 3, pp. 296–310, Sep. 2010.
- [16] W.-K. Kuo, S. Kumar, and C.-C. J. Kuo, “Improved priority access, bandwidth allocation and traffic scheduling for DOCSIS cable networks,” *IEEE Trans. Broadcasting*, vol. 49, no. 4, pp. 371–382, Dec. 2003.
- [17] D. B. Lee, H. Joo, and H. Song, “An effective channel control algorithm for integrated IPTV services over DOCSIS CATV networks,” *IEEE Transactions on Broadcasting*, vol. 53, no. 4, pp. 789–796, Dec 2007.
- [18] W. Liao, “The behavior of TCP over DOCSIS-based CATV networks,” *IEEE Trans. Commun.*, vol. 54, no. 9, pp. 1633–1642, Sep. 2006.
- [19] J. Martin and J. Westall, “A simulation model of the DOCSIS protocol,” *Simulation*, vol. 83, no. 2, pp. 139–155, Feb. 2007.
- [20] N. P. Shah, D. D. Kouvatso, J. Martin, and S. Moser, “On the performance modelling and optimisation of DOCSIS HFC networks,” in *Net. Perf. Eng., LNCS, Vol. 5233*, D. D. Kouvatso, Ed. Springer, Berlin, Germany, 2011, pp. 682–715.
- [21] S.-T. Sheu and M.-H. Chen, “A new network architecture with intelligent node (IN) to enhance IEEE 802.14 HFC networks,” *IEEE Transactions on Broadcasting*, vol. 45, no. 3, pp. 308–317, Sep. 1999.
- [22] J. Wang and J. Speidel, “Packet acquisition in upstream transmission of the DOCSIS standard,” *IEEE Transactions on Broadcasting*, vol. 49, no. 1, pp. 26–31, Mar 2003.
- [23] C.-Y. Chang, R. Schiavi, N. Nikaein, T. Spyropoulos, and C. Bonnet, “Impact of packetization and functional split on C-RAN fronthaul performance,” in *Proc. IEEE ICC*, 2016, pp. 1–7.
- [24] A. Checko, H. L. Christiansen, Y. Yan, L. Scolari, G. Kardaras, M. S. Berger, and L. Dittmann, “Cloud RAN for mobile networks—A technology overview,” *IEEE Communications Surveys & Tutorials*, vol. 17, no. 1, pp. 405–426, First Qu. 2015.
- [25] N. Fernando, S. W. Loke, and W. Rahayu, “Mobile cloud computing: A survey,” *Future Generation Computer Systems*, vol. 29, no. 1, pp. 84–106, Jan. 2013.
- [26] J. Liu, S. Zhou, J. Gong, Z. Niu, and S. Xu, “Statistical multiplexing gain analysis of heterogeneous virtual base station pools in cloud radio access networks,” *IEEE Trans. Wireless Commun.*, vol. 15, no. 8, pp. 5681–5694, Aug. 2016.
- [27] M. Peng, Y. Sun, X. Li, Z. Mao, and C. Wang, “Recent advances in cloud radio access networks: System architectures, key techniques, and open issues,” *IEEE Communications Surveys & Tutorials*, vol. 18, no. 3, pp. 2282–2308, Third Qu. 2016.

- [28] J. Wu, Z. Zhang, Y. Hong, and Y. Wen, "Cloud radio access network (C-RAN): A primer," *IEEE Network*, vol. 29, no. 1, pp. 35–41, Jan.-Feb. 2015.
- [29] S.-C. Zhan and D. Niyato, "A coalition formation game for remote radio head cooperation in cloud radio access network," *IEEE Trans. Vehicular Technol.*, vol. 66, no. 2, pp. 1723–1738, Feb. 2017.
- [30] K. Miyamoto, S. Kuwano, J. Terada, and A. Otaka, "Analysis of mobile fronthaul bandwidth and wireless transmission performance in split-PHY processing architecture," *OSA Opt. Expr.*, vol. 24, no. 2, pp. 1261–1268, Jan. 2016.
- [31] K. Miyamoto, S. Kuwano, T. Shimizu, J. Terada, and A. Otaka, "Performance evaluation of ethernet-based mobile fronthaul and wireless CoMP in split-PHY processing," *IEEE/OSA J. Opt. Commun. and Netw.*, vol. 9, no. 1, pp. A46–A54, Jan. 2017.
- [32] F. Tonini, M. Fiorani, M. Furdek, L. Wosinska, C. Raffaelli, and P. Monti, "Minimum cost deployment of radio and transport resources in centralized radio architectures," in *Proc. Int. Conf. on IEEE Comp., Netw. and Commun. (ICNC)*, 2016, pp. 1–5.
- [33] D. Boviz, A. Gopalasingham, C. S. Chen, and L. Roullet, "Physical layer split for user selective uplink joint reception in SDN enabled cloud-RAN," in *Proc. IEEE Australian Commun. Theory Workshop (AusCTW)*, 2016, pp. 83–88.
- [34] C.-Y. Chang, N. Nikaiein, R. Knopp, T. Spyropoulos, and S. S. Kumar, "FlexCRAN: A flexible functional split framework over Ethernet fronthaul in Cloud-RAN," in *Proc. IEEE ICC*, 2017, pp. 1–6.
- [35] U. Dötsch, M. Doll, H.-P. Mayer, F. Schaich, J. Segel, and P. Sehier, "Quantitative analysis of split base station processing and determination of advantageous architectures for LTE," *Bell Labs Technical Journal*, vol. 18, no. 1, pp. 105–128, Jun. 2013.
- [36] A. Maeder, M. Lalam, A. De Domenico, E. Pateromichelakis, D. Wubben, J. Bartelt, R. Fritzsche, and P. Rost, "Towards a flexible functional split for cloud-RAN networks," in *Proc. IEEE Int. Conf. Networks and Commun.*, 2014, pp. 1–5.
- [37] G. Mountaser, M. L. Rosas, T. Mahmoodi, and M. Dohler, "On the feasibility of MAC and PHY split in cloud RAN," in *Proc. IEEE Wireless Commun. and Netw. Conf. (WCNC)*, 2017, pp. 1–6.
- [38] N. Makris, P. Basaras, T. Korakis, N. Nikaiein, and L. Tassiulas, "Experimental evaluation of functional splits for 5G Cloud-RANs," in *Proc. IEEE ICC*, 2017, pp. 1–6.
- [39] N. Nikaiein, E. Schiller, R. Favraud, R. Knopp, I. Alyafawi, and T. Braun, "Towards a cloud-native radio access network," in *Adv. in Mobile Cloud Comp. and Big Data in the 5G Era*, C. Mavroumoustakis, G. Matorakis, and C. Dobre, Eds. Springer, Cham, Switzerland, 2017, pp. 171–202.
- [40] S. Nishihara, S. Kuwano, K. Miyamoto, J. Terada, and A. Ootaka, "Study on protocol and required bandwidth for 5G mobile fronthaul in C-RAN architecture with MAC-PHY split," in *Proc. IEEE Asia-Pacific Conf. on Communications (APCC)*, 2016, pp. 1–5.
- [41] L. Wang and S. Zhou, "On the fronthaul statistical multiplexing gain," *IEEE Commun. Letters*, vol. 21, no. 5, pp. 1099–1102, May 2017.
- [42] X. Wang, A. Alabbasi, and C. Cavdar, "Interplay of energy and bandwidth consumption in CRAN with optimal function split," in *Proc. IEEE ICC*, 2017, pp. 1–6.
- [43] A. De Domenico, E. C. Strinati, and A. Capone, "Enabling green cellular networks: A survey and outlook," *Computer Communications*, vol. 37, pp. 5–24, Jan. 2014.
- [44] M. Fiorani, S. Tombaz, F. S. Farias, L. Wosinska, and P. Monti, "Joint design of radio and transport for green residential access networks," *IEEE J. Sel. Areas in Commun.*, vol. 34, no. 4, pp. 812–822, Apr. 2016.
- [45] B. Kantarci and H. T. Mouftah, "Energy efficiency in the extended-reach fiber-wireless access networks," *IEEE Network*, vol. 26, no. 2, pp. 28–35, Mar.-Apr. 2012.
- [46] —, "Designing an energy-efficient cloud network [invited]," *IEEE/OSA Journal of Optical Communications and Networking*, vol. 4, no. 11, pp. B101–B113, Nov. 2012.
- [47] E. Oh, K. Son, and B. Krishnamachari, "Dynamic base station switching-on/off strategies for green cellular networks," *IEEE Transactions on Wireless Communications*, vol. 12, no. 5, pp. 2126–2136, May 2013.
- [48] L. Suarez, L. Nuaymi, and J.-M. Bonnin, "An overview and classification of research approaches in green wireless networks," *EURASIP J. on Wireless Commun. and Netw.*, vol. 2012, no. 142, pp. 1–18, 2012.
- [49] J. Wu, Y. Zhang, M. Zukerman, and E. K.-N. Yung, "Energy-efficient base-stations sleep-mode techniques in green cellular networks: A survey," *IEEE Commun. Surv. & Tut.*, vol. 17, no. 2, pp. 803–826, Second Qu. 2015.
- [50] Z. Zhu, "A novel energy-aware design to build green broadband cable access networks," *IEEE Communications Letters*, vol. 15, no. 8, pp. 887–889, Aug. 2011.
- [51] —, "Design of energy-saving algorithms for hybrid fiber coaxial networks based on the DOCSIS 3.0 standard," *IEEE/OSA Jour. of Optical Commun. and Net.*, vol. 4, no. 6, pp. 449–456, June 2012.
- [52] P. Lu, Y. Yuan, Z. Yang, and Z. Zhu, "On the performance analysis of energy-efficient upstream scheduling for hybrid fiber-coaxial networks with channel bonding," *IEEE Commun. Letters*, vol. 17, no. 5, pp. 1020–1023, May 2013.
- [53] X. Li, X. Wang, K. Li, and V. Leung, "CaaS: Caching as a service for 5G networks," *IEEE Access*, vol. 5, pp. 5982–5993, 2017.
- [54] R. G. Stephen and R. Zhang, "Green OFDMA resource allocation in cache-enabled CRAN," in *Proc. IEEE Online Conference on Green Commun. (OnlineGreenComm)*, Nov. 2016, pp. 70–75.
- [55] Z. Zhao, M. Peng, Z. Ding, W. Wang, and H. V. Poor, "Cluster content caching: An energy-efficient approach to improve quality of service in cloud radio access networks," *IEEE J. Sel. Areas in Commun.*, vol. 34, no. 5, pp. 1207–1221, May 2016.
- [56] J. Gambini, S. Savazzi, P. Castiglione, U. Spagnolini, and G. Matz, "Wireless over cable in femtocell systems: A case study from indoor channel measurements," in *Proc. IEEE Wireless Commun. and Net. Conf. Wksp.*, Apr. 2012, pp. 137–141.
- [57] J. Gambini and U. Spagnolini, "LTE femtocell system through amplify-and-forward over cable links," in *Proc. IEEE Globecom Wkshps*, 2010, pp. 716–720.
- [58] J. P. Pereira and P. Ferreira, "Infrastructure sharing as an opportunity to promote competition in local access networks," *Journal of Computer Networks and Communications*, vol. 2012, no. 409817, pp. 1–11, 2012.
- [59] W. Briglauer, S. Frühling, and I. Vogelsang, "The impact of alternative public policies on the deployment of new communications infrastructure—a survey," *Review of Network Economics*, vol. 13, no. 3, pp. 227–270, Sep. 2014.
- [60] H. Gruber, J. Hätönen, and P. Koutroumpis, "Broadband access in the EU: An assessment of future economic benefits," *Telecommunications Policy*, vol. 38, no. 11, pp. 1046–1058, Dec. 2014.
- [61] J. Schneir and Y. Xiong, "Cost analysis of network sharing in FTTH/PONs," *IEEE Commun. Mag.*, vol. 52, no. 8, pp. 126–134, Aug. 2014.
- [62] N. Becker, A. Rizk, and M. Fidler, "A measurement study on the application-level performance of LTE," in *Proc. IEEE/IFIP Networking Conf.*, 2014, pp. 1–9.
- [63] C. Studer and G. Durisi, "Quantized massive MU-MIMO-OFDM uplink," *IEEE Trans. Commun.*, vol. 64, no. 6, pp. 2387–2399, Jun. 2016.
- [64] A. Pitarokoilis, E. Björnson, and E. G. Larsson, "Performance of the massive MIMO uplink with OFDM and phase noise," *IEEE Communications Letters*, vol. 20, no. 8, pp. 1595–1598, Aug. 2016.
- [65] CableLabs, "Distributed CCAP architectures overview technical report," Louisville, CO, Sep. 2015.
- [66] K. Sundaresan, "Evolution of CMTS/CCAP architectures," in *INTX Spring Techn. Forum Proc.*, May 2015.
- [67] S. He and M. Torkelson, "Designing pipeline FFT processor for OFDM (de) modulation," in *Proc. IEEE URSI Int. Symp. on Signals, Systems, and Electronics (ISSSE)*, 1998, pp. 257–262.
- [68] M. Khelifi, D. Massicotte, and Y. Savaria, "Parallel independent FFT implementation on Intel processors and Xeon Phi for LTE and OFDM systems," in *Proc. Nordic Circuits and Systems Conf. (NORCAS): NORCHIP & Int. Symp. on System-on-Chip (SoC)*, 2015, pp. 1–4.
- [69] —, "Towards efficient and concurrent FFTs implementation on Intel Xeon/MIC clusters for LTE and HPC," in *Proc. IEEE Int. Symp. on Circuits and Systems (ISCAS)*, 2016, pp. 2611–2614.
- [70] L. Ma, R. D. Chamberlain, K. Agrawal, C. Tian, and Z. Hu, "Analysis of classic algorithms on highly-threaded many-core architectures," *Future Generation Computer Systems*, in print, 2017.
- [71] E. Wang, Q. Zhang, B. Shen, G. Zhang, X. Lu, Q. Wu, and Y. Wang, "Intel math kernel library," in *High-Performance Computing on the Intel® Xeon Phi™*. Springer, Cham, Switzerland, 2014, pp. 167–188.
- [72] I.-G. Jang and G.-D. Jo, "Study on the latency efficient IFFT design method for low latency communication systems," in *Proc. IEEE Int. Symp. Intelligent Signal Proc. and Commun. Sys.*, 2016, pp. 1–4.
- [73] Y.-J. Kim, I.-G. Jang, K.-J. Cho, and J.-G. Chung, "Low-latency and memory-efficient SDF IFFT processor design for 3GPP LTE," *IEICE Electronics Express*, vol. 14, no. 12, pp. 1–6, 2017.

- [74] K. Fukuoka, O. Ozawa, R. Mori, Y. Igarashi, T. Sasaki, T. Kuraishi, Y. Yasu, and K. Ishibashi, "A 1.92 μ s-wake-up time thick-gate-oxide power switch technique for ultra low-power single-chip mobile processors," in *Proc. IEEE Symp. on VLSI Circuits*, 2007, pp. 128–129.
- [75] T. Fukuda, K. Kohara, T. Dozaka, Y. Takeyama, T. Midorikawa, K. Hashimoto, I. Wakiyama, S. Miyano, and T. Hojo, "A 7ns-access-time 25 μ W/MHz 128kb SRAM for low-power fast wake-up MCU in 65nm CMOS with 27fA/b retention current," in *IEEE Int. Solid-State Circuits Conf. Digest of Techn. Papers (ISSCC)*, 2014, pp. 236–237.
- [76] Z. Hu, A. Buyuktosunoglu, V. Srinivasan, V. Zyuban, H. Jacobson, and P. Bose, "Microarchitectural techniques for power gating of execution units," in *Proc. ACM Int. Symp. on Low Power Electronics and Design*, 2004, pp. 32–37.
- [77] K.-I. Kawasaki, T. Shiota, K. Nakayama, and A. Inoue, "A sub- μ s wake-up time power gating technique with bypass power line for rush current support," *IEEE Journal of Solid-State Circuits*, vol. 44, no. 4, pp. 1178–1183, Apr. 2009.
- [78] G. C. Buttazzo, "Rate monotonic vs. EDF: Judgment day," *Real-Time Systems*, vol. 29, no. 1, pp. 5–26, Jan. 2005.
- [79] R. R. Howell and M. K. Venkatrao, "On non-preemptive scheduling of recurring tasks using inserted idle times," *Information and Computation*, vol. 117, no. 1, pp. 50–62, Feb. 1995.
- [80] M. Joseph and P. Pandya, "Finding response times in a real-time system," *The Computer Journal*, vol. 29, no. 5, pp. 390–395, Jan. 1986.
- [81] I. Shin and I. Lee, "Compositional real-time scheduling framework with periodic model," *ACM Transactions on Embedded Computing Systems (TECS)*, vol. 7, no. 3, pp. 30:1–30:39, Apr. 2008.
- [82] C. L. Liu and J. W. Layland, "Scheduling algorithms for multiprogramming in a hard-real-time environment," *Journal of the ACM (JACM)*, vol. 20, no. 1, pp. 46–61, Jan. 1973.
- [83] K. Jeffay, D. F. Stanat, and C. U. Martel, "On non-preemptive scheduling of period and sporadic tasks," in *Proc. IEEE Real-Time Systems Symposium*, 1991, pp. 129–139.
- [84] T. P. Baker and A. Shaw, "The cyclic executive model and Ada," *Real-Time Systems*, vol. 1, no. 1, pp. 7–25, Jun. 1989.
- [85] L. Sha and J. B. Goodenough, "Real-time scheduling theory and ada," DTIC Document, CMU/SEL-88-TR-033, ESD-TR-88-034, Tech. Rep., Nov. 1988.
- [86] J. Li, L. Shu, J.-J. Chen, and G. Li, "Energy-efficient scheduling in nonpreemptive systems with real-time constraints," *IEEE Trans. Sys., Man, and Cybernetics: Sys.*, vol. 43, no. 2, pp. 332–344, Mar. 2013.
- [87] J. Lin, A. M. Cheng, and W. Song, "A practical framework to study low-power scheduling algorithms on real-time and embedded systems," *J. Low Power Electr. and Appl.*, vol. 4, no. 2, pp. 90–109, 2014.
- [88] L. Niu and W. Li, "Energy-efficient scheduling for embedded real-time systems using threshold work-demand analysis," *Journal of Circuits, Systems and Computers*, vol. 26, no. 06, pp. 1 750 091–1–1 750 091–36, Jun. 2017.
- [89] L. Yu, F. Teng, and F. Magoules, "Node scaling analysis for power-aware real-time tasks scheduling," *IEEE Transactions on Computers*, vol. 65, no. 8, pp. 2510–2521, Aug. 2016.
- [90] A. Nirmalathas, P. A. Gamage, C. Lim, D. Novak, and R. Waterhouse, "Digitized radio-over-fiber technologies for converged optical wireless access network," *IEEE/OSA Journal of Lightwave Technology*, vol. 28, no. 16, pp. 2366–2375, Aug. 2010.
- [91] D. Novak, R. B. Waterhouse, A. Nirmalathas, C. Lim, P. A. Gamage, T. R. Clark, M. L. Dennis, and J. A. Nanzer, "Radio-over-fiber technologies for emerging wireless systems," *IEEE Journal of Quantum Electronics*, vol. 52, no. 1, pp. 1–11, Jan. 2016.
- [92] S. Rajpal and R. Goyal, "A review on radio-over-fiber technology-based integrated (optical/wireless) networks," *Journal of Optical Communications*, vol. 38, no. 1, pp. 19–25, Jun. 2017.
- [93] N. Ghazisaidi and M. Maier, "Fiber-wireless (FiWi) networks: Technologies, architectures, and future challenges," in *Convergence of Mobile and Stationary Next-Generation Networks*, K. Iniewski, Ed. John Wiley & Sons, Inc., Hoboken, NJ, 2010, pp. 109–140.
- [94] —, "Fiber-wireless (FiWi) access networks: Challenges and opportunities," *IEEE Network*, vol. 25, no. 1, pp. 36–42, Jan.-Feb. 2011.
- [95] T. Tsagklas and F. Pavlidou, "A survey on radio-and-fiber FiWi network architectures," *Journal of Selected Area in Telecommunications (JSAT)*, pp. 18–24, Mar. 2011.
- [96] F. Aurzada, M. Lévesque, M. Maier, and M. Reisslein, "FiWi access networks based on next-generation PON and gigabit-class WLAN technologies: A capacity and delay analysis," *IEEE/ACM Transactions on Networking*, vol. 22, no. 4, pp. 1176–1189, Aug. 2014.
- [97] A. S. Thyagaturu, A. Mercian, M. P. McGarry, M. Reisslein, and W. Kellerer, "Software defined optical networks (SDONs): A comprehensive survey," *IEEE Communications Surveys & Tutorials*, vol. 18, no. 4, pp. 2738–2786, Fourth Qu. 2016.
- [98] "CPRI specification eCPRI 1.0, common public radio interface," 2017. [Online]. Available: http://www.cpri.info/downloads/eCPRI_v_1_0_2017_08_22.pdf
- [99] A. De la Oliva, J. A. Hernández, D. Larrabeiti, and A. Azcorra, "An overview of the CPRI specification and its application to C-RAN-based LTE scenarios," *IEEE Commun. Mag.*, vol. 54, no. 2, pp. 152–159, Feb. 2016.
- [100] X. Liu, H. Zeng, N. Chand, and F. Effenberger, "CPRI-compatible efficient mobile fronthaul transmission via equalized TDMA achieving 256 Gb/s CPRI-equivalent data rate in a single 10-GHz-bandwidth IM-DD channel," in *Proc. IEEE/OSA OFC*, 2016, pp. 1–3.
- [101] "Open base station architecture initiative," 2017. [Online]. Available: <http://www.obsai.com/>
- [102] CableLabs, "Data-over-cable service interface specifications, remote downstream external PHY interface specification," Jan 2016.
- [103] —, "Remote upstream external PHY interface specification, data-over-cable service interface specifications," Jan 2016.
- [104] S.-H. Cho, H. Park, H. S. Chung, K.-H. Doo, S. S. Lee, and J. H. Lee, "Cost-effective next generation mobile fronthaul architecture with multi-IF carrier transmission scheme," in *Proc. OSA Optical Fiber Commun. Conf.*, 2014, pp. Tu2B–6–1–Tu2B–6–3.
- [105] B. G. Kim, S. Bae, H. Kim, and Y. Chung, "Mobile fronthaul optical link for LTE-A system using directly-modulated 1.5- μ m VCSEL," in *Proc. IEEE Int. OptoElectronics and Commun. Conf.*, 2016, pp. 1–3.
- [106] N. Nikaein, "Processing radio access network functions in the cloud: Critical issues and modeling," in *Proc. ACM Int. Wkshps on Mobile Cloud Computing and Services*, 2015, pp. 36–43.
- [107] J.-S. Joung, J.-H. Lee, L. Yong-Hoon, H.-J. Lee, and C.-W. Yoo, "Base station apparatus for decreasing amount of transmission data with cloud radio access network," May 28 2013, US Patent App. 13/903,333.
- [108] "ETSI TS 36.211, Evolved Universal Terrestrial Radio Access (E-UTRA): Physical channels and modulation," 2017. [Online]. Available: <https://portal.3gpp.org/desktopmodules/Specifications/SpecificationDetails.aspx?specificationId=2425>
- [109] "The spectral efficiency of DOCSIS 3.1 systems," 2013. [Online]. Available: https://www.arris.com/globalassets/resources/white-papers/arris_spectral_efficiency_of_docsis_wp.pdf
- [110] M. M. Mansour and L. M. Jalloul, "Optimized configurable architectures for scalable soft-input soft-output MIMO detectors with 256-QAM," *IEEE Trans. Signal Proc.*, vol. 63, no. 18, pp. 4969–4984, Sep. 2015.
- [111] M. P. McGarry, M. Reisslein, F. Aurzada, and M. Scheutzwow, "Shortest propagation delay (SPD) first scheduling for EPONs with heterogeneous propagation delays," *IEEE J. on Sel. Areas in Commun.*, vol. 28, no. 6, pp. 849–862, Aug. 2010.
- [112] S. Y. Choi, S. Lee, T.-J. Lee, M. Y. Chung, and H. Choo, "Double-phase polling algorithm based on partitioned ONU subgroups for high utilization in EPONs," *IEEE/OSA J. Opt. Commun. Netw.*, vol. 1, no. 5, pp. 484–497, Oct. 2009.
- [113] A. Mercian, M. P. McGarry, and M. Reisslein, "Offline and online multi-thread polling in long-reach PONs: A critical evaluation," *IEEE/OSA Journal of Lightwave Technology*, vol. 31, no. 12, pp. 2018–2028, Jun. 2013.
- [114] A. Mercian, E. I. Gurrola, F. Aurzada, M. P. McGarry, and M. Reisslein, "Upstream polling protocols for flow control in PON/xDSL hybrid access networks," *IEEE Transactions on Communications*, vol. 64, no. 7, pp. 2971–2984, Jul. 2016.
- [115] M. Agiwal, A. Roy, and N. Saxena, "Next generation 5G wireless networks: A comprehensive survey," *IEEE Commun. Surveys & Tutorials*, vol. 18, no. 3, pp. 1617–1655, Third Qu. 2016.
- [116] M. H. Alsharif and R. Nordin, "Evolution towards fifth generation (5G) wireless networks: Current trends and challenges in the deployment of millimetre wave, massive MIMO, and small cells," *Telecommunication Systems*, vol. 64, no. 4, pp. 617–637, Apr. 2017.
- [117] S. Gosselin, A. Pizzinat, X. Grall, D. Breuer, E. Bogenfeld, S. Krauß, J. A. T. Gijón, A. Hamidian, N. Fonseca, and B. Skubic, "Fixed and mobile convergence: Which role for optical networks?" *IEEE/OSA Journal of Optical Commun. and Netw.*, vol. 7, no. 11, pp. 1075–1083, Nov. 2015.
- [118] S. I. Goudar, S. Hassan, and A. Habbal, "5G: The next wave of digital society challenges and current trends," *Journal of Telecommunication, Electronic and Computer Engineering (JTEC)*, vol. 9, no. 1-2, pp. 63–66, 2017.

- [119] R. Brenot and G. De Valicourt, "Telecommunications network node linking a metropolitan area network with at least one access network," Jan. 3 2017, US Patent 9,537,597.
- [120] M. Maier, M. Reisslein, and A. Wolisz, "A hybrid MAC protocol for a metro WDM network using multiple free spectral ranges of an arrayed-waveguide grating," *Computer Networks*, vol. 41, no. 4, pp. 407–433, Mar. 2003.
- [121] M. Scheutzow, M. Maier, M. Reisslein, and A. Wolisz, "Wavelength reuse for efficient packet-switched transport in an AWG-based metro WDM network," *IEEE J. Lightwave Techn.*, vol. 21, no. 6, pp. 1435–1455, Jun. 2003.
- [122] H.-S. Yang, M. Maier, M. Reisslein, and W. M. Carlyle, "A genetic algorithm-based methodology for optimizing multiservice convergence in a metro WDM network," *IEEE/OSA Journal of Lightwave Technology*, vol. 21, no. 5, pp. 1114–1133, May 2003.
- [123] A. X. Zheng, L. Zhang, and V. W. Chan, "Metropolitan area network architecture for optical flow switching," *IEEE/OSA Journal of Optical Communications and Networking*, vol. 9, no. 6, pp. 511–523, Jun. 2017.
- [124] M. Jaber, M. A. Imran, R. Tafazolli, and A. Tukmanov, "5G backhaul challenges and emerging research directions: A survey," *IEEE Access*, vol. 4, pp. 1743–1766, 2016.
- [125] K. S. Munasinghe, I. Elgendi, A. Jamalipour, and D. Sharma, "Traffic offloading 3-tiered SDN architecture for DenseNets," *IEEE Network*, vol. 31, no. 3, pp. 56–62, May/June 2017.
- [126] A. S. Thyagaturu, Y. Dashti, and M. Reisslein, "SDN-based smart gateways (Sm-GWs) for multi-operator small cell network management," *IEEE Transactions on Network and Service Management*, vol. 13, no. 4, pp. 740–753, Dec. 2016.

PLACE
PHOTO
HERE

Akhilesh Thyagaturu is an Engineer at Intel Mobile Communications, San Diego, CA, USA, and an Adjunct Faculty in the School of Electrical, Computer, and Energy Engineering at Arizona State University (ASU), Tempe. He received the Ph.D. in electrical engineering from Arizona State University, Tempe, in 2017. He serves as reviewer for various journals including the *IEEE Communications Surveys & Tutorials*, *IEEE Transactions of Network and Service Management*, and *Optical Fiber Technology*. He was with Qualcomm Technologies Inc., San Diego, CA, USA, as an Engineer from 2013 to 2015.

PLACE
PHOTO
HERE

Ziyad Alharbi is a researcher at King Abdulaziz City for Science and Technology (KACST), Riyadh, Saudi Arabia. He received his B.Sc. degree in Electrical Engineering from King Fahd University of Petroleum and Minerals, Saudi Arabia, and his M.S. in Electrical Engineering from Arizona State University, Tempe. Currently, he is working towards his Ph.D. in Electrical Engineering at Arizona State University. He serves as reviewer for various journals including *IEEE Communications Surveys & Tutorials*, *Computer Networks*, and *Optical Switching*

and *Networking*

PLACE
PHOTO
HERE

Martin Reisslein (A'96-S'97-M'98-SM'03-F'14) is a Professor in the School of Electrical, Computer, and Energy Engineering at Arizona State University (ASU), Tempe. He received the Ph.D. in systems engineering from the University of Pennsylvania in 1998. He currently serves as Associate Editor for the *IEEE Transactions on Mobile Computing*, the *IEEE Transactions on Education*, and *IEEE Access* as well as *Computer Networks* and *Optical Switching and Networking*. He is Associate Editor-in-Chief for the *IEEE Communications Surveys & Tutorials* and chairs the steering committee of the *IEEE Transactions on Multimedia*.

chairs the steering committee of the *IEEE Transactions on Multimedia*.